МІНІСТЕРСТВО ОСВІТИ ТА НАУКИ УКРАЇНИ
НАЦІОНАЛЬНИЙ АВІАЦІЙНИЙ УНІВЕРСИТЕТ
КАФЕДРА КОНСТРУКЦІЇ ЛІТАЛЬНИХ АПАРАТІВ

ДОПУСТИТИ ДО ЗАХИСТУ
Завідувач кафедри, д.т.н., проф.
_____ Сергій ІГНАТОВИЧ
«_____» _____ 2021 р.

ДИПЛОМНА РОБОТА
ВИПУСКНИКА ОСВІТНЬОГО СТУПЕНЯ МАГІСТРА
ЗІ СПЕЦІАЛЬНОСТІ
«АВІАЦІЙНА ТА РАКЕТНО-КОСМІЧНА ТЕХНІКА»

Тема: «Аванпроект середньомагістрального вузькофюзеляжного пасажирського літака місткістю до 200 пасажирів»

Виконавець: _____ **У Цзюнькан**

Керівник: к. т. н., доц. _____ **В.С. Краснопольський**

Консультанти з окремих розділів пояснювальної записки:
охорона праці:
к. біол. н., доц. _____ **Вікторія КОВАЛЕНКО**

охорона навколишнього середовища:
к. т. н., доц. _____ **Тамара ДУДАР**

Нормоконтролер: к. т. н, доц. _____ **Сергій ХИЖНЯК**

Київ 2021

MINISTRY OF EDUCATION AND SCIENCE OF UKRAINE
NATIONAL AVIATION UNIVERSITY
DEPARTMENT OF AIRCRAFT DESIGN

PERMISSION TO DEFEND
Head of the department,
Professor, Dr. of Sc.
_____Sergiy IGNATOVYCH
«___» _____ 2021

MASTER DEGREE THESIS
ON SPECIALITY
“AVIATION AND ROCKET-SPACE ENGINEERING”

Topic: «Preliminary design of the mid-range narrow-body passenger aircraft with up to 200 passengers capacity »

Fulfilled by: _____ **Wu Junkang**

Supervisor:
PhD, associate professor _____ **V.S. KRASNOPOLSKII**

Labor protection advisor:
PhD, associate professor _____ **Victoria KOVALENKO**
Environmental protection adviser:
Ph.D. associate professor _____ **Tamara DUDAR**

Standards inspector
Ph.D. associate professor _____ **Sergiy KHIZNYAK**

Kyiv 2021

НАЦІОНАЛЬНИЙ АВІАЦІЙНИЙ УНІВЕРСИТЕТ

Аерокосмічний факультет
Кафедра конструкції літальних апаратів
Освітній ступінь «Магістр»
Спеціальність 134 «Авіаційна та ракетно-космічна техніка»
Освітньо-професійна програма «Обладнання повітряних суден»

ЗАТВЕРДЖУЮ
Завідувач кафедри, д.т.н, проф.
_____ Сергій ІГНАТОВИЧ
«_____» _____ 2021 р.

ЗАВДАННЯ
на виконання дипломної роботи студента
У Цзюнькан

1.Тема:«Ескізний проект середньомагістрального вузькофюзеляжного пасажирського літака вмісністю до 200 пасажирів», затверджений наказом ректора №815/ст. «21» травня 2021 року.

2. Строки дипломної роботи: з 01.10.2021 року по 05.12.2021 року.

3. Вихідні дані: крейсерська швидкість Vcr = 835 км/год, дальність польоту L = 4075 км, робоча висота Hor = 10,5 км.

4. Зміст: вступ; основна частина: аналіз дослідних зразків та короткий опис проектування літака, вибір вихідних даних, розрахунок геометрії крила та компонування літака, конструкція шасі, вибір двигуна, розрахунок центру ваги, спеціальна частина: Чисельне дослідження пошкодження конструкції літака MSD, праці охорона, Охорона навколишнього середовища.

5. Необхідний матеріал: загальний вигляд літака, макет літака.

6. Календарний план-графік

№ пор.	Завдання	Термін виконання	Відмітка про виконання
1	Отримання завдання, обробка статистичних даних.	5.10.2021–9.10.2021	
2	Визначення злітної маси літака та розрахунок льотних характеристик.	9.10.2021–13.10.2021	

3	Визначення центрування літака.	13.10.2021–4.10.2021	
4	Графічний дизайн літака та його компонування.	14.11.2021–17.11.2021	
5	Проаналізуйте дані та розрахуйте модель.	17.11.2021-20.11.2021	
6	Охорона праці .	20.11.2020–23.11.2020	
7	Охорона навколишнього середовища.	23.11.2020–26.11.2020	
8	Підготовка ілюстративного матеріалу, написання доповіді.	26.11.2021–29.11.2021	
9	Перевірка редагування та виправлення пояснювальної записки.	30.11.2021–6.12.2021	

7. Консультанти з окремих розділів:

Розділ	Консультант	Дата, підпис	
		Завдання видав	Завдання прийняв
Охорона праці	к.біол.н., доцент Вікторія КОВАЛЕНКО		
Охорона навколишнього середовища	к.т.н, доцент Тамара ДУДАР		

8. Дата видачі завдання: 8 жовтня 2021 року

Керівник дипломної роботи _____ В.С. Краснопольський
(підпис керівника) П.І.Б.

Завдання прийняв до виконання _____ У Цзюнькан
(підпис студента) П.І.Б.

NATIONAL AVIATION UNIVERSITY

Faculty ____Aerospace_____
Department __of Aircraft Design__
Educational degree __«Master»__
Specialty 134 "Aviation and space rocket technology"
Educational program __"Aircraft equipment"__

APPROVED BY
Head of department
D.Sc., professor
_____ S.R. Ignatovych
«___» _____ 2021.

TASK
for the master thesis
Wu Junkang

1. Topic: «Preliminary design of the mid-range narrow-body passenger aircraft with up to 200 passengers capacity» approved by the Rector's order №815/ст. «21» May 2021 year.
2. Thesis terms: since 01.10.2021 year till 05.12.2021 year.
3. Initial data: cruise speed V_{cr} = 835 km/h, flight range L = 4075 km, operating altitude H_{op} = 10.5 km.
4. Content: introduction; main part: analysis of prototypes and brief description of designing aircraft, selection of initial data, wing geometry calculation and aircraft layout, landing gear design, engine selection, center of gravity calculation, special part: Numerical Study on MSD Damage of Aircraft Structure, Labor protection, Environmental protection.
5. Required material: general view of the airplane, layout of the airplane.
6. Thesis schedule

№	Task	Time limits	Done
1	Task receiving, processing of statistical data.	5.10.2021–9.10.2021	
2	Aircraft take-off mass determination and flight performances calculation.	9.10.2021–13.10.2021	
3	Aircraft centering determination.	13.10.2021–14.10.2021	
4	Graphical design of the aircraft and its layout.	14.11.2021–17.11.2021	
5	Analyze the data and calculate the model.	17.11.2021-20.11.2021	
6	Labor protection .	20.11.2020– 23.11.2020	
7	Environmental protection.	23.11.2020– 26.11.2020	

8	Preparation of illustrative material, writing the report.	26.11.2021–29.11.2021	
9	Explanatory note checking, editing and correction.	30.11.2021–06.12.2021	

7. Special chapter advisers:

Chapter	Adviser	Date, signature	
		Task issued	Task received
Labor protection	PhD, associate professor Victoria KOVALENKO		
Environmental protection	PhD, associate professor Tamara DUDAR		

8.Date: «6» December 2021 year.

Supervisor _____ V.S. Krasnopolskii

Student _____ Wu Junkang

РЕФЕРАТ

Магістерська робота «Ескізний проект середньомагістрального вузькофюзеляжного пасажирського літака вмісністю до 200 пасажирів»

59 сторінок, 11 рисунків, 9 таблиць, 21 посилання

Об'єкт дослідження – процес проектування цивільного літака.

Предмет дослідження – ескізний проект середньомагістрального вузькофюзеляжного пасажирського літака місткістю до 200 пасажирів.

Мета магістерської роботи – створити ескізний проект літака та оцінити його льотні характеристики.

Методи дослідження та розробки - Метод проектування ґрунтується на аналізі прототипу, виборі найбільш передових технічних рішень та інженерних розрахунків та отриманні технічних даних проектованого літака. У спеціальній частині проведено чисельний аналіз та теоретичні дослідження обшивки салону літака на основі теорії багатоточкової втоми ушкоджень.

Новизна результатів - досліджено правило зміни коефіцієнта взаємного впливу між поширенням тріщини в обшивці літака, а потім досліджено правило взаємного поширення тріщини.

Практична цінність – результати роботи можуть бути використані в авіаційній галузі та в процесі навчання авіаційної професійної підготовки.

ПАСАЖИРСЬКИЙ ЛІТАК, ЕШЕДІЙНИЙ ПРОЕКТ, РОЗРАХУНОК ЦЕНТРА ГРАВІТАЦІЇ, ЗАКОН РОСТУ ТРІЩИН

ABSTRACT

Master thesis « Preliminary design of the mid-range narrow-body passenger aircraft with up to 200 passengers capacity »

59 pages, 11 figures, 9 tables, 21 references

Object of study – design process of a civil airplane.

Subject of study – is preliminary design of the mid-range narrow-body passenger aircraft with up to 200 passengers capacity.

Aim of master thesis – is to create a preliminary design of an airplane and estimate its flight performances.

Research and development methods - The design method is based on prototype analysis, selecting the most advanced technical decisions and engineering calculations, and obtaining the technical data of the designed aircraft. In the special part, numerical analysis and theoretical research on the aircraft cabin skin are carried out based on the multi-point damage fatigue theory.

Novelty of the results - the change rule of the mutual influence factor between the crack propagation in the aircraft skin is studied, and then the mutual propagation rule of the crack is explored.

Practical value - work results can be used in the aviation industry and aviation professional education process.

PASSENGER AIRCRAFT, PRELIMINARY DESIGN, CENTER OF GRAVITY CALCULATION, CRACK GROWTH LAW

CONTENT

INTRODUCTION

Aircraft structure must take into account both functionality and economy, and require light weight, long life, high reliability, and good safety. This makes the aircraft structure design increasingly complex, fatigue problems more prominent, and more difficult to use and maintain. Aviation fatigue is one of the key factors that affect the performance of the aircraft under development/service, and seriously affects the maneuverability, reliability and safety of the aircraft. In order to meet the severe requirements of the aircraft's service environment and the high-performance technical index requirements in the development of new models, the research on aviation fatigue issues needs to run through the entire life cycle of aircraft development and operation, and should be given key consideration and attention.

The goal of this project is to design a medium-range narrow-body passenger aircraft capable of accommodating less than 200 people, and to study the fatigue characteristics of its cabin skin based on the multi-point fatigue damage theory, and to give certain research value and reference basis in engineering design.

1. PROJECT PART. PRELIMINARY DESIGN OF MID RANGE AIRCRAFT

1.1 Analysis of prototypes and short description of designed aircraft

Aircraft design begins with a series of design requirements and design specifications. For example, performance indicators require that the aircraft is capable of flying a long enough distance (that is, to meet the range requirements) at a certain speed with a rated load. The calculation of aircraft related parameters is a very important task whether it is in the conceptual design stage, the preliminary design stage, or the detailed design stage. Therefore, in the overall design stage of the aircraft, the size and weight of each main component must be estimated reasonably and accurately, so as to weigh the plan. And optimized design provides a reliable basis.

In the early stage of conceptual design, in order to meet the requirements of a given mission and estimate the performance of the aircraft, it is necessary to estimate the maximum take-off weight (MTOW) of the aircraft. Then the maximum take-off weight is broken down into several main weight data: used empty weight, fuel weight, and load weight. Using the empirical formula, the empty weight can be further decomposed into the structural weight of each component. The structural weight of each component can be calculated with a more refined method to calculate a more accurate structural weight. Accurate weight data can help designers make correct decisions and improve design quality. Therefore, it is very necessary to accurately calculate the weight of the aircraft. In the early stages of aircraft design, only a few overall aircraft parameters are known, such as maximum take-off weight, range, lift-to-drag ratio, etc. Many detailed information cannot be known. Without knowing the detailed data, the designer cannot calculate the weight, but can only estimate the weight. With the advancement of the design process, more and more detailed information can be learned, and the weight estimation is gradually decreasing, and the weight calculation is gradually increasing. When the design enters the final stage and the prototype has been produced, the weight of the aircraft and its components can be measured, which can verify

the correctness of the weight estimation or calculation. The prototype of the aircraft designed in the work carried out in this article is C919, and the statistical data of the performances of prototypes are presented in Table 1.1.

Table 1.1

Performances of prototype – C919

Parameter	**Value**
The purpose of airplane	Passenger
Crew/flight attend. persons	2/5
Maximum take-off weight, m_{tow}, kg	97413
Maximum payload, $m_{k.max}$, kg	22021
Passenger's seat	190
The flight altitude, $V_{w.ex.}$, m	10.5
Range, $m_{k.max}$, km	4075
Take-off distance, $L_{t.d.}$, m	1725
Number and type of engines	2XLEAP-X1C
Aspect Ratio	10.00
Taper Ratio	3.0
Sweepback angle at 1/4 chord line, ^{0}	28

1.2 Brief description of the main parts of the aircraft

1.2.1 Wing

The wing of the C919 is a wing with a special wing profile (wing profile). The fixed-wing aircraft with this airfoil design can greatly improve aerodynamic performance in the transonic range, reduce drag and improve attitude controllability.

The supercritical wing adopts a wing with a special wing profile (airfoil). It can increase the critical Mach number of the wing and delay the occurrence of the rapid increase in the resistance of the wing at high subsonic speeds. Its airfoil is called a supercritical airfoil and was first proposed by R.T. Whitcomb in 1967. Its shape is characterized by the front

edge being blunt and rounded compared to the ordinary airfoil, the upper surface is flat, the lower surface is close to the trailing edge, there is an anti-concave, the trailing edge is thin, and it is curved downward. When the airflow bypasses the leading edge of the ordinary airfoil, the speed increases more (the sharper the leading edge, the greater the angle of attack, and the more the increase), and the flow velocity on the upper surface of the airfoil continues to increase. The greater the thickness of the airfoil, the higher the upper surface bulges, and the more the speed increases. When the flying speed is high enough (equivalent to a Mach number of 0.85～0.9), the local flow velocity on the upper surface of the airfoil can reach the speed of sound. The flying Mach number at this time is called the critical Mach number. When the flight speed increases again, a strong shock wave will appear on the upper surface, causing the airflow to separate, and the wing resistance increases sharply. In order to maintain the economy of airplane flight, the flying Mach number should not exceed the critical Mach number. To increase the flight speed, we must try to increase the critical Mach number of the wing. Reducing the thickness of the wing or adopting a swept-back wing (see swept-wing aircraft) can increase the critical Mach number, but this will increase the weight of the wing. The use of supercritical wing can increase the critical Mach number without having to pay the price of increasing the weight of the wing.

The leading edge of the supercritical airfoil is blunt, and the velocity increases less when the air flows around, and the flat upper surface makes the local velocity change little. In this way, only when the flying Mach number is high, the local airflow on the upper surface reaches the speed of sound, that is, the critical Mach number is high. After reaching the speed of sound, the local airflow speed increases slowly, the shock wave formed is weaker, the drag increases slowly, and the lift characteristics are better.

Supercritical wings can also be used to reduce the weight of aircraft structures. If a high-subsonic aircraft with swept wings uses supercritical wings, while maintaining the same flight speed, straight wings can be used while the wing thickness remains the same, so that the weight of the wing can be reduced. At the same time, the low-speed aerodynamic characteristics of the wings are improved. If you maintain the same sweep angle and use a thick wing, you can also reduce the weight of the wing, and increase the volume in the wing

to place fuel or other equipment.

1.2.2 Fuselage

The C919 passenger aircraft is a short- and medium-haul commercial aircraft with an actual total length of 38 meters, a wingspan of 35.8 meters, and a height of 12 meters. Its basic layout is 168 seats. The cabin seat layout will adopt a single aisle, with three seats on each side, and the middle seat space will be widened, effectively alleviating the crowded feeling of passengers in the middle seat in the past. According to official information, C919 adopts advanced environmental control and lighting design, providing passengers with larger observation windows, better cabin space, and better comfort for passengers; at the same time, the section perimeter is reduced by 0.326% and the section area is reduced by 0.711. %, the weight of the fuselage structure is reduced by 26.7kg.

1.2.3 Tail unit

The tail unit consists of horizontal and vertical stabilizers, elevators and rudders. In addition, the skin at the tail cone of the aircraft is equipped with a skin deflector to prevent the combustible power leaving the aircraft from entering the auxiliary power unit (APU) tail nozzle.

1.2.4 Landing gear

The first three-point landing gear is used on the C919 aircraft. The two main wheels are arranged symmetrically behind the center of mass of the aircraft at a certain distance, and the front wheels are arranged under the nose of the aircraft. When the aircraft is taxiing and parking on the ground, the fuselage floor is basically in a horizontal position, which is convenient for passengers to board the aircraft and load and unload cargo. In order to meet the needs of aircraft take-off, landing roll and ground taxiing, the lower end of the landing gear is equipped with wheels with pneumatic tires. For shorten the landing roll distance, brakes or automatic braking devices are installed on the wheels. In addition, it also includes load-bearing struts, shock absorbers (usually load-bearing struts are used as shock absorber outer cylinders), retractable mechanism, front wheel damper and turning control mechanism.

The load-bearing strut connects the wheel and the shock absorber to the airframe, and transmits the impact load during landing and taxiing to the airframe. The front wheel damper is used to eliminate the shimmy of the front wheel during high-speed coasting. The front wheel turning control mechanism can increase the flexibility of the aircraft's ground turning.

1.2.5 Control system

The cockpit is the cockpit where the pilot controls the airplane. Except for some early airplanes, the cockpit of most airplanes nowadays adopts a closed design. The cockpit of the airplane is generally equipped with various flight instruments and aircraft control systems. The flight system of the C919, a large passenger aircraft with independent intellectual property rights developed in accordance with international standards for the first time in my country, is at the world’s leading level. Sidestick operation technology similar to the A320 series. The overhead panel is divided into a front top panel and a rear top panel. Including flight control system switch components, navigation signal source and display switch components, ventilation system switch components, power system switch components, wiper switch, light brightness, windshield and wing deicing switch components, night light switch, APU start switch, engine Start switch, etc. Equipped with EFIS control panel and FCU control panel, with main warning and attention lights on both sides. The main flight display screen contains the main flight attitude, heading and route information, weather information, oil and gas circuit information, etc. All the screens can be switched, as a backup for each other. In the middle are the spare horizon and landing gear selector handles. The system integrated display contains other important information directly related to the flight, such as ground instructions and cabin environment information. Center console (front): Contains engine throttle, flaps, communication frequency information, etc. Central console (rear): Contains switches such as brake lever, cockpit door lock, ram air turbine switch, etc. In addition, the operating system, power distribution system and display system of the C919 cockpit can be said to have drawn advanced technologies from Boeing and Airbus.

The C919 cockpit operating system mainly includes side sticks, active side sticks and throttle platforms. This system has been tested and used by test pilots and pilots for nearly 30 years. At present, there are approximately 12,000 aircraft using similar systems in the

world. The improved flight control system has high reliability and maturity. In addition, a major feature of the C919 flight control system is the pilot's flight situation awareness system using active feed technology, which can avoid the pilot's perception of environmental factors in time and space during flight.

The C919's power distribution system is similar to the Boeing 787 Dreamliner. It uses a solid-state power controller (SSPC), eliminating the need for low-reliability components, improving the reliability of the aircraft. The power distribution unit containing the solid-state power controller can be deployed on the entire aircraft and remotely controlled, which can minimize the total wiring requirements of the aircraft and reduce the weight of the aircraft.

1.2.6 Onboard equipment

The C919 cockpit display system uses the most advanced integrated display technology. Contains five 15.4-inch large-screen displays. The five displays are in a T-shaped layout. They can simultaneously provide the main flight data (speed, altitude, attitude, etc.), navigation, communication, monitoring, electronic checklist, weather and Information such as terrain and other system working status. The five LCD screens are in a T-shaped layout, replacing the traditional instrument panel. Compared with ordinary civil aircraft display systems, the C919 not only has a larger display area, but also displays more content. Many airplanes in the same seat class use "small" displays ranging from 8 inches to 10 inches, and much of the content is displayed separately, and a single display only displays a certain type of information. However, C919 adopts "comprehensive display" technology. All kinds of display information are processed by software to achieve a high degree of integration. It can display multiple types of data on one monitor, and multiple monitors can be switched with each other. good. The integrated display technology of C919 is comparable to Boeing B787 and Airbus A350XWB, reaching the international advanced technology level.

1.2.7 Choice and description of power plant

The LEAP-X1C engine uses carbon fiber composite fan blades developed by France's SNECMA company and ceramic matrix composite turbine components developed by General Electric Company of the United States. The LEAP-X1C engine will have 18 fan blades, which is half the number of CFM56-5C and three-quarters of CFM56-7B. COMAC chose the complete integrated propulsion system (IPS) provided by GE and France's Safran for the C919. The engine uses many leading innovative technologies in the industry, including ultra-high pressure ratio core machines, composite fan blades manufactured using three-dimensional braided resin mold transfer molding technology, a unique debris removal system, composite fan casings, and third 3D aerodynamic design compressor and turbine blade design technology; second-generation dual-ring premixed cyclone (TAPS Ⅱ) combustor technology using 3D printed fuel nozzles, high-pressure turbocomposite casing using ceramic matrix composites, variable area exterior Culvert nozzles, low-pressure turbines using lightweight titanium aluminide blades, and other advanced materials. The engine and nacelle are designed as an integrated propulsion system, with advanced air intake, acoustic treatment and electric thrust reverser, which can give full play to its aerodynamic performance, weight and acoustic advantages.

The engine's fan is an advanced carbon fiber composite fan blade, which can effectively reduce noise and improve propulsion efficiency. The number of fan blades is 18, the diameter is 1.8 meters, and the total weight is 76 kg. The thrust level of the engine is 89~134kN; the core engine has an 8-stage compressor, a single-stage high-pressure turbine and an advanced second-generation dual-ring premixed cyclone combustor. It has a simpler and more compact structure, lighter weight, stronger bearing capacity and higher efficiency for compressors and turbines, and more advanced engine regulation and control systems. In order to significantly reduce weight, the edge of the engine's fan blades is made of titanium alloy, and the blade itself is a composite fan blade manufactured by using three-dimensional braided resin mold transfer molding technology. This innovative technology using carbon fiber and a special manufacturing process creates a maintenance-free, extremely durable fan blade. The test results show that the blades made with this technology are not only light in weight, but also strong in structure, strong in resistance to large-volume bird strikes, and

relatively low manufacturing costs.

1.3 Geometry calculations for the main parts of the aircraft

Layout of the aircraft is determined by relative disposition of its parts and structures and requires the calculation of all types of loads caused by passengers, cargo, fuel and so on. The choice of the scheme, composition and aircraft parameters is directed to the best meets the operational requirements.

1.3.1 Wing geometry calculation

Geometrical characteristics of the wing are determined from the take-off weight m_0 and specific wing load p_0.

Full wing area with extensions is:

$$S_w = \frac{m_0 \cdot g}{p_0} = \frac{97413 \cdot 9.8}{5065} = 188.48 \text{ m}^2,$$

where S_w – wing area, m^2; g – acceleration due to gravity m/s^2.

Relative wing extensions area is 0.01.

Wing span is:

$$l = \sqrt{S_w \cdot \lambda_w} = \sqrt{188.48 \cdot 10} = 43.4 \text{ m},$$

where l – wing span, m; λ_w – wing aspect ratio.

Root chord is:

$$b_0 = \frac{2S_w \cdot \eta_w}{(1+\eta_w) \cdot l} = \frac{2 \cdot 188.48 \cdot 3}{(1+3) \cdot 43.4} = 6.514 \text{ m},$$

where b_0 – root chord, m; η_w – wing taper ratio.

Tip chord is:

$$b_t = \frac{b_0}{\eta_w} = \frac{6.514}{3} = 2.17 \text{ m},$$

where b_t – tip chord, m.

Maximum wing thickness is determined in the forehead i-section and is equal to:

$$c_i = c_w \cdot b_t = 0.12 \cdot 2.17 = 0.26 \text{ m},$$

where c_i – wing thickness in i-section, m; c_w – related wing thickness.

On board chord for trapezoidal shaped wing is:

$$b_b = b_0 \cdot \left(1 - \frac{(\eta_w - 1) \cdot D_f}{\eta_w \cdot l_w}\right) = 6.514 \cdot \left(1 - \frac{(3-1) \cdot 4.2}{3 \cdot 43.4}\right) = 6.09 \text{ m},$$

where b_b – wing board chord, m; D_f – fuselage diameter, m.

For mean aerodynamic chord determination the geometrical method was used (fig. 1.1). The geometrical method implies the measuring of parallel to the chords line which lies on the intersection of the section connecting the middles of tip and root chords with another section connecting the upper end of tip chord extension (which is equal to the length of root chord) with lower end of root chord extension (which is equal to the length of the tip chord). This method was chosen due to accuracy and simplicity in performance. Mean aerodynamic chord is equal to b_{MAC} = 4.65m.

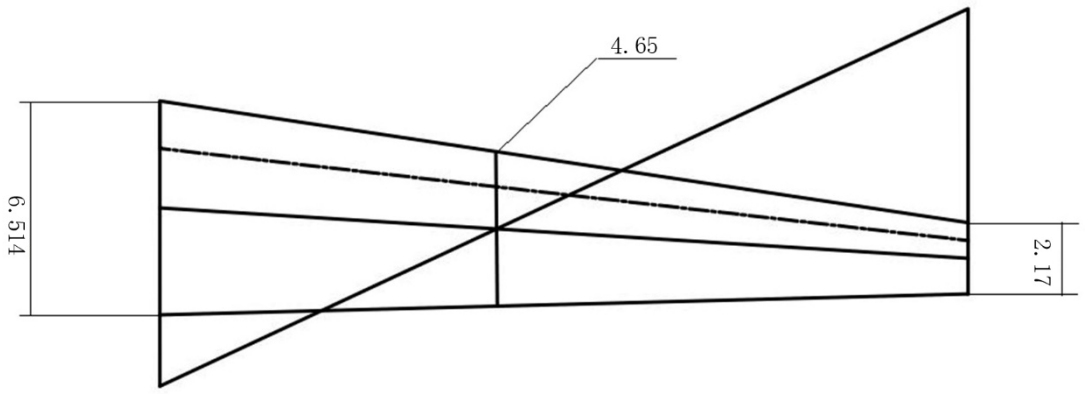

Fig. 1.1. Determination of mean aerodynamic chord.

After the size of the wing is determined, the aileron area is then calculated. The aileron area should account for about 5-20% of the wing area, and its length should be between 30-80% of the wing. The values are as follows:

$$l_{ail} = 0.35 \cdot \frac{l}{2} = 0.35 \cdot \frac{43.4}{2} = 7.595 \text{ m},$$

where l_{ail} – ailerons span, m.

Aileron area is:

$$S_{ail} = 0.07 \cdot \frac{S_w}{2} = 0.07 \cdot \frac{188.48}{2} = 6.60 \text{ m}^2,$$

where S_{ail} – ailerons area, m.

Increasing of l_{ail} and b_{ail} more than recommended values is not necessary and convenient. With the increase of l_{ail} more than given value the increase of the ailerons coefficient falls, and the high-lift devices span decreases. With b_{ail} increase, the width of the wing chord decreases.

To choose the structural scheme, hinge-fitting scheme and kinematics of the high-lift devices it is needed to take into account the statistics and experience of native and foreign aircraft designs. Have to be mentioned that in the majority of existing designs of high-lift devices they are made by spar structural scheme.

1.3.2 Fuselage layout

The layout of the fuselage is closely related to the shape and structure of the aircraft and the layout of large components, and the dynamic characteristics of the aircraft and the aerodynamic forces received. It is related to the flight characteristics and performance of the aircraft. Application of circular shape of fuselage nose part significantly minimize its drag:

$$l_{fnp} = 1.5 \cdot D_f = 1.5 \cdot 4.2 = 6.3 \text{ m},$$

where D_f – fuselage diameter, m; l_{fnp} – length of fuselage nose part.

Except aerodynamic requirements it is necessary to consider the strength and layout requirements. To geometrical parameters used in calculation are: fuselage diameter D_f, fuselage length l_f, fuselage aspect ratio λ_f, fuselage nose part aspect ratio λ_{np}. Fuselage length is determined considering the aircraft scheme, layout and airplane center-of-gravity position peculiarities and landing angle of attack α_{land}.

Fuselage length is equal to:

$$l_f = \lambda_f \cdot D_f = 9.3 \cdot 4.2 = 39.06 \text{ m}.$$

Fuselage nose part aspect ratio is equal to:

$$\lambda_{fnp} = \frac{l_{fnp}}{D_f} = \frac{6.3}{4.2} = 1.5.$$

Length of the fuselage rear part is equal to:

$$l_{frp} = \lambda_{frp} \cdot D_f = 3.03 \cdot 4.2 = 12.73 \text{ m}.$$

During the determination of fuselage length it is necessary to get minimum mid-section on the one hand and meet layout demands on the other.

For passenger airplanes fuselage mid-section first of all depends on the size of passenger cabin. One of the main parameter that determines the mid-section of passenger airplane is the height of the passenger cabin.

Cabin height is equal to:

$$H_{cab} = 1.48 + 0.17 \cdot B_{cab} = 1.48 + 0.17 \cdot 4.2 = 2.194 \text{ m},$$

where H_{cab} – cabin height, m; B_{cab} – width of the cabin, m.

C919 has three cabin layout configurations: full economy class, mixed class and high-density class. The full economy class has 168 seats; the mixed class has 156 seats, the business class has 12 seats in 3 rows, and the economy class has 144 seats; the high-density class has 180 seats, business class. The cabin has 4 seats in each row, and the economy class

has 6 seats in each row; there are a total of 4 attendant seats, 2 in the front service area, and 2 in the rear service area.

The width of the cabin in the economic class where seats are located in one row (4+6) is:

$$B_{cab} = n_3 b_3 + n_{aisle} \cdot b_{aisle} + 2\delta = 3 \cdot 0.78 + 5 \cdot 0.32 + 2 \cdot 0.05 = 3.96 \text{ m},$$

where n_3 – number of three-seat blocks; b_3 – width of three-seat blocks, m; n_{aisle} – number of aisles; b_{aisle} – width of aisle, m; δ – distance between external armrests to the decorative panels, m.

The length of passenger cabin is equal to:

$$L_{cab} = L_1 \left(n_{rows} - 1\right) \cdot L_{sp} + L_2 = 0.9 \cdot \left(52 - 1\right) \cdot 0.84 + 0.35 = 38.9 \text{ m},$$

where L_{cab} – length of passenger cabin, m; L_1 – distance from the wall to the back of the seat in first row, m; L_2 – distance from the back of the seat in last row to the wall, m; n_{rows} – number of rows; L_{sp} – seat pitch, m.

1.3.3 Luggage compartment

Given the fact that the unit load on floor K = 600-800 kg/m^2

The area of cargo compartment is:

$$S_{cargo} = \frac{M_{bag}}{0.4K} + \frac{M_{c\&m}}{0.6K} = \frac{5000}{0.4 \cdot 600} + \frac{1200}{0.6 \cdot 800} = 23.5 \text{ m}^2,$$

where S_{cargo} – cargo compartment volume, m^3; M_{bag} – mass of the baggage, kg; $M_{c\&m}$ – mass of the cargo and mail, kg.

Cargo compartment volume is equal to:

$$\nu_{cargo} = \nu_c \cdot n_{pass} = 0.2 \cdot 150 = 30 \text{ m}^3,$$

where ν_{cargo} – cargo compartment volume, m^3; ν_c – cargo volume coefficient, m^3; n_{pass} –

number of passengers. Luggage compartment design is similar to the prototype.

1.3.4 Galleys and buffets

International standards require two dishes for airplanes with mixed layout. Kitchen cupboards must be placed between the cockpit and passenger cabin. Refreshment and food can not be placed near the toilets and wardrobes. Volume of buffets and galleys is equal to:

$$\nu_{galley} = \nu_g \cdot n_{pass} = 0.1 \cdot 150 = 15\ \text{m}^3,$$

where ν_{galley} – galley volume, m^3; ν_g – galley volume coefficient, m^3; n_{pass} – number of passengers.

Area of buffets and galleys is equal to:

$$S_{galley} = \frac{\nu_{galley}}{H_{cab}} = \frac{15}{2.014} = 7.45\ \text{m}^2,$$

where S_{galley} – galley area, m^2.

Number of meals per passenger breakfast, lunch and dinner – 0,75 kg; tea and water – 0,45 kg. Passengers are fed every 3.5…4 hour of flight. Buffet design is similar to prototype.

1.3.5 Lavatories

Number of toilet facilities is determined by the number of passengers and flight duration: with t > 4:00 one toilet for 40 passengers. The number of lavatories is equal to:

$$n_{lav} = \frac{n_{pass}}{40} = \frac{160}{40} = 4$$

where n_{lav} – number of lavatories.

So the chosen number of lavatories is 4. Area of each lavatory is 1.6 m^2 and width – 1 m. Toilets design is similar to the prototype.

1.3.6 Layout and calculation of basic parameters of tail unit

The tail unit of the aircraft needs to calculate the geometric dimensions of the vertical and horizontal stabilizers and the dimensions of the control surface. Generally speaking, the tail unit must meet the requirements of aircraft stability and controllability.

Area of vertical tail unit is equal to:

$$S_{VTU} = \frac{l_w \cdot S_w}{L_{VTU}} \cdot A_{VTU} = \frac{43.4 \cdot 188.48}{15.2} \cdot 0.08 = 43 \text{ m}^2,$$

where S_{VTU} – area of vertical tail unit, m^2; L_{VTU} – length of vertical tail unit, m; A_{VTU} – coefficient of static moment of vertical tail unit.

Area o horizontal tail unit is equal to:

$$S_{HTU} = \frac{b_{MAC} \cdot S_w}{L_{HTU}} \cdot A_{HTU} = \frac{4.56 \cdot 188.48}{15.2} \cdot 0.8 = 45.235 \text{ m}^2,$$

where S_{HTU} – area of horizontal tail unit, m^2; L_{HTU} – length of horizontal tail unit, m; A_{HTU} – coefficient of static momentum of horizontal tail unit.

Values L_{HTU} and L_{VTU} depend on some factors. First of all their value are influenced by the length of he nose part and tail part of the fuselage, sweptback and wing location, and also from the conditions of stability and control of the airplane.

Altitude elevator area is:

$$S_{el} = k_{el} \cdot S_{HTU} = 0.35 \cdot 45.235 = 15.83 \text{ m}^2,$$

where S_{el} – elevator area, m^2; k_{el} – relative elevator area coefficient.

Rudder area is:

$$S_{rud} = k_r \cdot S_{VTU} = 0.4 \cdot 43 = 17.2 \text{ m}^2,$$

where S_{rud} – rudder area, m^2; k_r – relative rudder area coefficient.

Choose the area of aerodynamic balance:

$$0.3 \le M \le 0.6$$

$$S_{eb} = k_{eb} \cdot S_{el} = 0.22 \cdot 15.83 = 3.4826 \text{ m}^2,$$

$$S_{rb} = k_{rb} \cdot S_{rud} = 0.2 \cdot 17.2 = 3.42 \text{ m}^2,$$

where S_{eb} – area of elevator aerodynamic balance, m^2; S_{rb} – area of rudder aerodynamic balance, m^2; k_{eb} – relative elevator balance area coefficient; k_{rb} – relative rudder balance area coefficient.

The area of altitude elevator trim tab is:

$$S_{te} = k_{te} \cdot S_{el} = 0.1 \cdot 15.83 = 1.583 \text{ m}^2,$$

where S_{te} –elevator trim tab area, m^2; k_{te} – relative elevator trim tab area coefficient.

Area of rudder trim tab is:

$$S_{tr} = k_{tr} \cdot S_{rud} = 0.05 \cdot 17.2 = 0.86 \text{ m}^2,$$

where S_{tr} –rudder trim tab area, m^2; k_{tr} – relative trim tab area coefficient.

Root chord of horizontal stabilizer is:

$$b_{0HTU} = \frac{2 \cdot S_{HTU} \cdot \eta_{HTU}}{(1+\eta_{HTU}) \cdot L_{HTU}} = \frac{2 \cdot 45.235 \cdot 2.7}{(1+2.7) \cdot 15.2} = 4.343 \text{ m},$$

where η_{HTU} – horizontal tail unit taper ratio; b_{0HTU} – root chord of horizontal stabilizer, m.

Tip chord of horizontal stabilizer is:

$$b_{tHTU} = \frac{b_{0HTU}}{\eta_{HTU}} = \frac{4.343}{2.7} = 1.61 \text{ m},$$

where b_{tHTU} – tip chord of horizontal stabilizer, m.

Root chord of vertical stabilizer is:

$$b_{0VTU} = \frac{2 \cdot S_{VTU} \cdot \eta_{VTU}}{(1+\eta_{VTU}) \cdot L_{VTU}} = \frac{2 \cdot 43 \cdot 3}{(1+3) \cdot 15.2} = 4.243\text{m},$$

where b_{0VTU} – root chord of vertical stabilizer, m; η_{VTU} – vertical tail unit taper ratio; L_{VTU} – vertical tail unit span.

Tip chord of vertical stabilizer is:

$$b_{tVTU} = \frac{b_{0VTU}}{\eta_{VTU}} = \frac{4.243}{3} = 1.414\text{ m}.$$

where b_{tVTU} – tip chord of vertical stabilizer, m.

1.3.7 Landing gear design

To estimate the landing gear outline in this project it is necessary to calculate the location of every strut relatively to each other, to determine the loads on landing gear system, and its location considering centre of gravity of an airplane. In this layout the principal scheme of landing gear is fully based on the prototype data.

As in the case with the tail unit it is necessary to provide the aircraft with the stable and controllable base during operation on the ground including landing and take-off.

Main wheel axes offset is:

$$e = k_e \cdot b_{MAC} = 0.18 \cdot 4.65 = 0.837\text{ m},$$

where k_e – coefficient of axes offset; e – main wheel axes offset, m.

With the large wheel axial offset the lift-off of the front gear during take of is complicated and with small the drop of the airplane on the tail is possible when the loading of the back of the airplane comes first.

Landing gear wheel base is:

$$B = k_b \cdot l_f = 0.35 \cdot 39.06 = 13.671\text{m},$$

where B – wheel base, m; k_b – wheel base calculation coefficient.

Front wheel axial offset is:

$$d_n = B - e = 13.671 - 0.837 = 12.834 \text{ m},$$

where d_n – nose wheel axes offset, m.

Wheel track is:

$$T = k_T \cdot B = 0.8 \cdot 13.671 = 10.9368 \text{ m},$$

where T – wheel track, m; k_T – wheel track calculation coefficient.

Wheels for the landing gear is chosen by the size and run loading on it from the take-off weight. For the front support it is necessary to consider dynamic loading as well.

Type of the pneumatics (balloon, half balloon, arched) and the pressure in it is determined by the runway surface, which should be used. There are breaks on the main wheel.

Nose wheel load is:

$$P_n = \frac{g \cdot e \cdot k_d \cdot m_0}{B \cdot z} = \frac{9.8 \cdot 0.837 \cdot 1.75 \cdot 97413}{13.671 \cdot 2} = 51141 \text{ N},$$

where P_n – nose wheel load, N; k_d – dynamics coefficient; z – number of wheels.

Main wheel load is equal to:

$$P_m = \frac{\text{g} \cdot (B - e) \cdot m_0}{B \cdot n \cdot z} = \frac{9.8 \cdot 12.834 \cdot 97413}{13.671 \cdot 2 \cdot 4} = 112025\text{N},$$

where P_m – main wheel load, N; n – number of main landing gear struts.

According the calculated values of wheel loading and take-off speed it is possible choose the tires for landing gear from the catalog:

for nose landing gear

Aircraft Rib 461B-3434-TL with parameters $P_{rated} = 9000 \text{ lbf}$; $V_{rated} = 250 \text{ MPH}$; size 18×5.7-8.

for main landing gear

Aircraft Rib 461B-2728-TL with parameters $P_{rated} = 12000\,\text{lbf}$; $V_{rated} = 195\,MPH$; size 22×7.75-10.

The rate of wheel loading is:

for nose wheel $\frac{9000 - 8835}{9000} \cdot 100\% = 1.83\%$;

for main wheel $\frac{12000 - 11593}{12000} \cdot 100\% = 3.39\%$.

The values are less than 10% so choosed tires can be used for this airplane.

1.4 Center of gravity calculation

1.4.1 Trim-sheet of the equipped wing

Mass of the equipped wing contains the mass of its structure, mass of the equipment located in the wing and mass of the fuel. Regardless of the place of mounting (to the wing or to the fuselage) the main landing gear and the front gear are included in the mass register of the equipped wing. The mass register includes names of the objects, mass themselves and their center of gravity coordinates. The origin of the given coordinates of the mass centers is chosen by the projection of the nose point of the mean aerodynamic chord (MAC) for the surface XOY. The positive meanings of the coordinates of the mass centers are accepted for the aft part of the aircraft.

The list of the mass objects for the aircraft, where the engines are located under the wing, included the names given in the table 1.3. Coordinates of the center of mass for the equipped wing are defined by the formula (1.1).

$$X'_w = \frac{\sum m'_i \cdot x_i}{\sum m'_i}, \qquad (1.1)$$

where X'_w – center of mass for equipped wing, m; m'_i – mass of a unit, kg; x_i – center of mass of the unit, m.

1.4.2 Trim-sheet of the equipped fuselage

Origin of the coordinates is chosen in the projection of the nose of the fuselage on the

horizontal axis. For the axis X the construction part of the fuselage is given. The list of the objects for the equipped fuselage, with engines are mounted under the wing, is given in table 1.4. The CG coordinates of the equipped fuselage are determined by formula (1.2).

$$X'_f = \frac{\sum m'_i \cdot x_i}{\sum m'_i} \tag{1.2}$$

where X'_f – center of mass for equipped fuselage, m; m'_i – mass of a unit, kg; x_i – center of mass of the unit, m.

Table 1.3

Trim sheet of equipped wing

N	Name	Mass		CG coordinates x_i (m)	Moment $m_i x_i$ (kgm)
		Units	total mass m_i (kg)		
1	Wing (structure)	0.13842	8139.05848	1.96395	16771.44099
2	Fuel system	0.0069	559. 052	1.98045	1084.7958
3	Airplane control, 30%	0.00169	151. 3319	2. 72610	354.00522
4	Electrical equipment, 10%	0.00337	253. 38930	0. 51243	120.2839315
5	Anti-ice system, 50%	0.0135	862. 817	0. 51432	395.7448987
6	Hydraulic systems, 70%	0.01492	886. 40738	2. 72610	2123.403677
7	Power plant	0.07129	5300.5972	1.09882	5143.40448
8	Equipped wing without landing gear and fuel	0.23120	16120.9584	1.584	26858.08233
9	Nose landing gear	0.004222	291.2984	-9. 87042	-2987.3925
10	Main landing gear	0.035869	2622.288406	2.761072	6577.605548
11	Fuel	0.25879	19263.1952	1.95694	33716.08795
12	Equipped wing	0.53591	38493.1159	1.69358	60366.38334

After the CG of fully equipped wing and fuselage is determined, the moment equilibrium equation (1.3) relatively to the fuselage nose can been made.

$$m_f X_f^{'} + m_w (X_{MAC} + x_w^{/}) = m_0 (X_{MAC} + C) \qquad (1.3)$$

where m_0 – aircraft take-off mass, kg; m_f – mass of fully equipped fuselage, kg; m_w – mass of fully equipped wing, kg; C – distance from MAC leading edge to the CG point determined by the designer.

From here we determined the wing MAC leading edge position relative to fuselage, means X_{MAC} value by formula:

$$X_{MAC} = \frac{m_f \cdot X_f^{'} + m_w \cdot X_w^{'} - m_0 \cdot C}{m_0 - m_w} = \frac{37294 \cdot 18.69 + 38493 \cdot 1.69 - 97413 \cdot 0.32}{97413 - 38493} = 12.406 \text{ m}.$$

Table 1.4

Trim sheet of equipped fuselage

№	Objects	Mass		Coordinates of CG	Moment (kgm)
		Units	Total (kg)		
1	Fuselage	0.09735	6998.8809	17.5935	123134.8111
2	Horizontal tail	0.01112	799.46128	29	23184.37712
3	Vertical tail	0.01097	788.67718	29	22871.63822
4	Radar	0.0032	230.0608	0.5	115.0304
5	Radio equipment	0.0024	172.5456	1.2	207.05472
6	Instrument panel	0.0056	402.6064	1.3	523.38832
7	Navigation equipment	0.0048	345.0912	1.2	414.10944
8	Lavatory 1, 2, galley 1	0.00615	442.1481	4	1768.5924
9	Lavatory 3, 4, galley 2	0.00615	442.1481	28	12380.1468
10	Aircraft control system 70%	0.00455	327.1177	17.5935	5755.145255
11	Hydro-pneumatic system 30%	0.00528	379.60032	24.6309	9349.897522
12	Electrical equipment 90%	0.02943	2115.84042	17.5935	37225.03843
13	Nontypical equipment	0.0037	266.0078	15.834	4211.967505
14	Operational items	0.02149	1545.00206	2	3090.00412
15	Load devices equipment	0.0083	596.7202	15.834	9448.467647
16	Lining and insulation	0.0073	524.826	17.5935	9233.526231

17	Air-conditioning system, 25%	0.00575	413.39	17.5935	7272.976965
18	Anti-ice system 25%	0.00575	413.39	28.1496	11636.76314
19	Passenger seats (business)	0.000867	62.332098	6	373.992588
20	Passenger seats (economic class)	0.015383	1105.945402	18.4	20349.3954
21	Seats of flight attendance	0.000433	31.130102	7.5	233.475765
22	Seats of pilot	0.0002167	15.5794298	2.4	37.39063152
23	Additional equipment	0.0031	222.8714	15.834	3528.945748
24	**Equipped fuel without payload**	**0.2592897**	**18641.37249**	**16.43366848**	**306346.1355**
25	Passengers(business)	0.008464	608.510816	6	3651.064896
26	Onboard meal	0.00158	113.59252	4	454.37008
27	Baggage cargo, mail	0.051	3666.594	15.834	58056.8494
28	Crew	0.00635	456.5269	6	2739.1614
29	Passengers(economy)	0.150236	10801.06698	18.4	198739.6325
30	TOTAL	0.4769197	37293.66371	18.6968187	569987.2138

1.4.3 Calculation of center of gravity positioning variants

The list of mass objects for centre of gravity variant calculation given in table 1.5 and center of gravity calculation options given in table 1.6, completes on the base of both previous tables.

Table 1.5

Calculation of CG positioning variants

Name	Mass, kg	Coordinates CG, m	Moment, kgm
Object	m_i	x_i	M_i
Equipped wing (without fuel and landing gear)	17253.47	17.812	268902.9616
Nose landing gear (extended)	298.366834	6.57295	1811.986894
Main landing gear (extended)	2559.301506	18. 07912	49907.0201
Fuel/fuel reserve	17855.25278	18.24580	343791.7083
Equipped fuselage (without payload)	16481.37249	16. 66843348	336406.1355
Passengers of business class	608.5108	6.231	3561.0648

Passengers of economy class	10180.00698	19.55	197388.5284
Baggage cargo, mail	365.594	15.9994	55680.8494
Crew	251. 33809	5.4898	1350.56028
Nose landing gear	288.366834	5. 21857	1767.060764
Main landing gear	2595.301506	19. 30721	44969.98643
Reserve fuel	2302.76	21.5	49304.82

Table 1.6

Airplanes CG position variants

№	Variants of the loading	Mass, kg	Moment of the mass, kgm	Centre of the mass, m	Centering
1	Take-off mass (LG extended)	97413	1240860.815	17. 72364644	0.227456346
2	Take-off mass (LG retracted)	97413	1294846.855	17. 05963724	0.284632523
3	Landing weight (LG extended)	53452.47599	956543.927	17. 45624504	0.281170505
4	Ferry version	53658.89569	950880.4128	17. 55848348	0.207207373
5	Parking version	37872.58103	697456.1041	17.13464664	0.191871768

Conclusion to the project part

In this part the main geometric dimensions and centering of designed aircraft were determined. That made the creation of the drawing outline possible.

During the calculation the main geometrical parameters caused by operational purpose, planned quantities of passengers, speed and altitude of flight, conditions of landing and take-off were considered. All obtained values meet requirements for the short range passenger aircrafts.

The centering of the designed aircraft was performed. Geometrical parameters almost match with chosen prototypes. That fact allows to make a conclusion that designed aircraft will successfully compete with another models on the chosen market segment.

Furthermore, the engine LEAP-X1C that meets the requirements considering efficiency for designed aircraft was chosen. Main peculiarities of basic section of an aircraft and their influence on outline creation were figured out.

2. SPECIAL PART. Numerical Study on MSD Damage of Aircraft Structure

2.1 MSD damage structure in aircraft

There are a large number of cracks in multi-site damage, which can affect and connect with each other in a short period of time, resulting in a rapid decline in the residual strength of the structure. In analyzing crack expansion and residual strength, the analysis of the SIF variation law of the stress strength factor of MSD crack is the prerequisite for MSD crack expansion, structural residual strength and fatigue life analysis and prediction. MsD damage contains a lot of cracks, belongs to the multi-crack structure, the interaction between cracks is very significant. When a crack is expanding, it will lead to the redistribution of local internal forces of the structure within a certain range, which in turn affects the variation of the expansion law of other cracks in the range. At present, the SIF analysis methods of MSD crack include the compound function method, the right function method, the boundary metaface, the boundary metaface, and the finite metaface method. For the connection structure with any distribution MSD crack, the finitenor method is mainly used for analysis.

This section selects the structure with the largest presence of aircraft structures and the most prone to MSD damage - the structural form of multiple rivet holes:

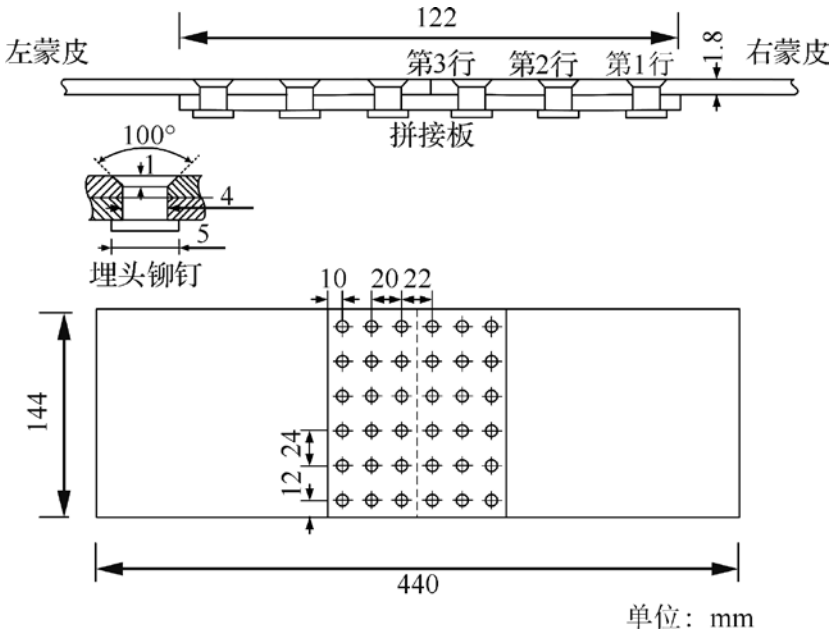

Figure2.1 MSD damaged structure-the structure of multiple rows of rivet holes

					NAU 21.08W.00.00.00.28 EN		
Done by	Wu Junkang					list	sheet	sheets
Supervisor	Krasnopolskii V.S.							
					Special part		
St.control.	Khyzhniak S.V.					ASF 603	
Head of dep.	Ignatovich S.R.						

The left and right skins are riveted with the splicing plate through 3 rows of 6 rivets. Skin thickness 1.8mm, splicing plate thickness 2.28mm, materials are 2024-T3 aluminum alloy. Rivet hole diameter of 4mm, rivets for buried rivets, material for 2117 aluminum alloy, rivets and holes for non-interference. The dimensions of the docking structure are shown in Figure 1, and the material properties are shown in Table 2.1.

Table2.1 Material properties

component	material	Elastic modulus/GPa	Yield strength/MPa	Tensile strength/MPa	Density kg/m^3
Skinning, splicing board	2024-T3	72.4	275	405	2780
rivet	2117	71.7			

2.2 FRANCO3D calculation process

This section uses FRANCO3D software for finitenum analysis of multi-position damage crack expansion. FRANC3D (FRacture ANalysis Code for 3D) is a new generation of crack analysis software developed by FAC Corporation of the United States to calculate the germination life of micro-fatigue cracks, including the germination and cracking direction of cracks, as well as the three-dimensional crack expansion and fatigue life of engineering structures in any complex geometry, load conditions, and crack patterns. The software defines the crack extension area as a submodel, remeshs the submodel, and then re-integrates the submodel with the crack and the remaining model for calculation, greatly increasing the speed of the calculation, and its workflow is shown in the figure2.2.

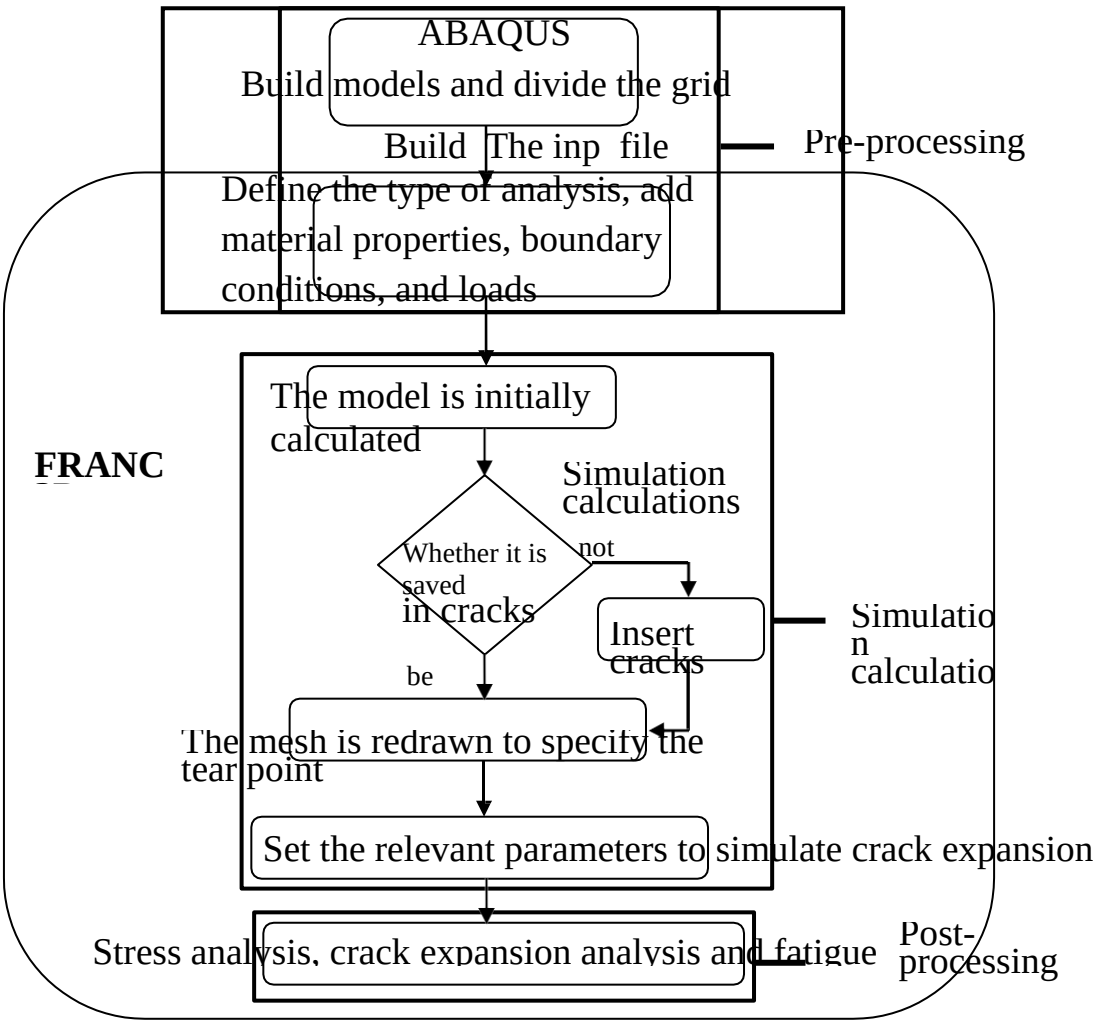

Figure2.2 FRANC3D simulates a crack stable expansion flowchart

The interaction of multi-crack tip is very complex, because the multi-site damage structure under the action of fatigue load, crack appears with great randomness, and the expansion of each crack is different, the load is constantly redistributed, the load value of each crack is constantly changing, the interaction between cracks is very serious. Therefore, this section will determine the interaction between cracks by means of crack tip interaction factors.

This article first looks at the different relative positions where cracks appear, and assumes:

(1) The cracks in the edges of each parallel hole are independent;

(2) The crack expansion model conforms to the Paris model;

(3) The crack produced by the symmetrical model under the action of pull-pull load is type I crack;

(4) Because the thickness of the metal plate is small relative to the size of the model (the

aspect ratio is 1%), the surface crack can be treated as a straight crack through.

2.3 Interaction factor calculation

In order to study the expansion of multi-position damage cracks, this section uses Franc3D to analyze the finitenum calculation of cracks in a variety of situations in two dimensions: hole edge crack expansion, hole edge conjoined crack expansion, and crack connectivity expansion. For ease of expression, number the fatigue details of the siding, as shown in the figure2.3.

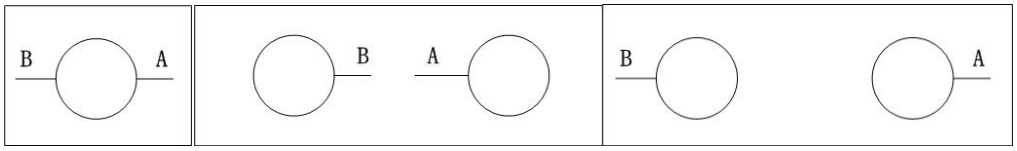

Mode 1 Mode 2 Mode 3

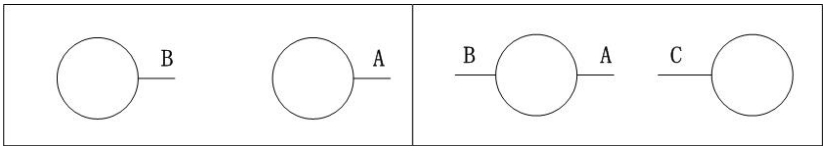

Mode 4 Mode 5

Figure2.3 Multi-site damage crack propagation mode

The computational requirements of the two-dimensional finite factor model are small, but it is difficult to consider factors such as sub-bending, rivet bending and warping, friction and so on in the riveting connection structure. With the development of finite-pupil simulation technology, Chen Yueliang and others, using the method of combining the three-dimensional model of the joining structure with the two-dimensional model of the joining area, studied the law of the change of the SIF in the thickness direction under the different crack lengths of the straight and sink hole edges. Zhang Teng et al. established a three-dimensional model of non-interfering riveting and bonding structure with MSD crack, and studied the change law of SIF in the thickness direction of MSD crack. Based on the three-dimensional model, Pitta et al. studied the SIF characteristics of the skin repair structure with crack riveting and fitting with crack.

In view of the MSD riveting butt structure, the distribution of SIF in the direction of crack tip thickness and the influence of splicing plate thickness and rivet shape are studied by using the three-dimensional finite factor model, which can provide reference for the design and analysis of the body skinning butt structure.

The load is applied according to the load at the time of the test, the lower end constrains the vertical displacement, the symmetry point constrains the lateral displacement to ensure that the model does not move horizontally, and the upper end applies the vertical tensile load. Since this paper is based on line elasticity research, the alternating load can be calculated according to static force and then converted into alternating load. The load spectrum is shown in the table2.2.

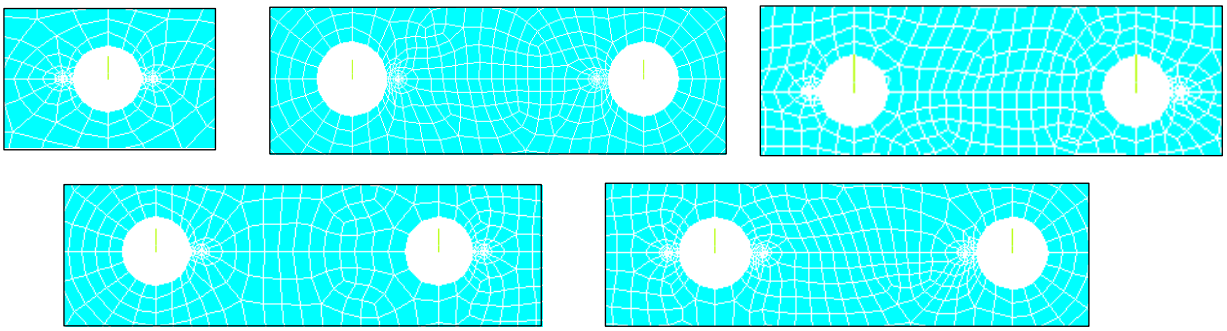

Figure2.4 The finite element model and the position distribution map of the five modes

Table2.2 load spectrum

Maximum Stress of The Hair Section (MPa)	Maximum load (kN)	Minimum stress on the gross cross section (MPa)	Minimum load (kN)	Stress Mean (MPa)	Stress amplitude (MPa)
85.3	136.4	5.1	8.18	40.1	45.2

The process of interaction between cracks is due to the local redistribution of forces in the structure, when a crack appears or expands, the crack will lose its carrying capacity, and the load it should bear will be assigned to other parts of the structure to bear, because the redistribution of the load crack expansion will change. Crack expansion is mainly to study the change law of stress intensity factors of cracks, this paper is to study the interaction between cracks by studying the change laws of stress intensity factors. Add a quantity that reflects the change of local internal forces to the expression that calculates the crack stress strength factor, and the expression of the stress strength factor becomes

$$K_I = \beta Y \sigma \sqrt{\pi a}$$

β is a local stress correction factor.

For structures with a single crack, the stress strength factor at the tip of the crack is marked K_0 and the expression of the stress strength factor is

$$K_0 = Y_0 \sigma \sqrt{\pi a}$$

$Y_{0(a)}$ depends on the geometry, crack form, and crack length of the structure, which is

the shape parameter of the crack, also known as the geometric configuration factor.

In an MSD structure, a component often contains many cracks. At this point, the interaction between cracks should be considered, and the expression of the stress strength factor is

$$K_i = \beta_i Y_{0i} \sigma \sqrt{\pi a_i} (i = 1, 2, ..., n)$$

Y_{0i} is the geometric configuration factor ofthe crack tip stress strength factor when the structure has only one crack ai; βi is the n that exists in the structure at the same time.The correction factor of a crack to a crack tip stress strength factor, which specifically reflects the interaction between cracks, and is called the interaction factor of the crack tip.

According to the above division of multi-site damage mode, the stress intensity factor solved in different modes under the experimental load by finite elements software, and on this basis, the interaction factors in different modes are solved according to the mutual influence factor solution method mentioned.

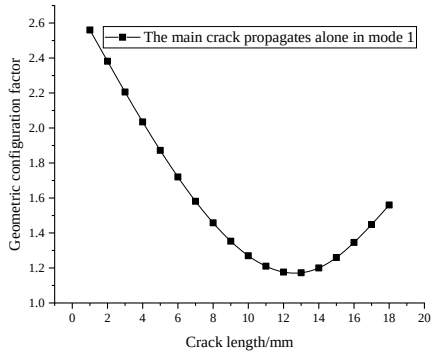

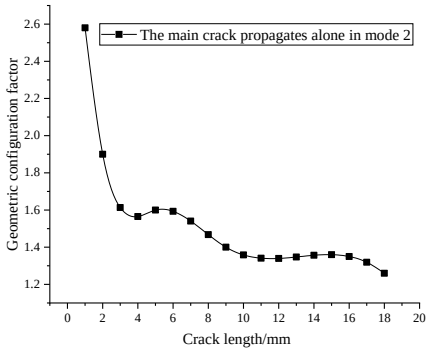

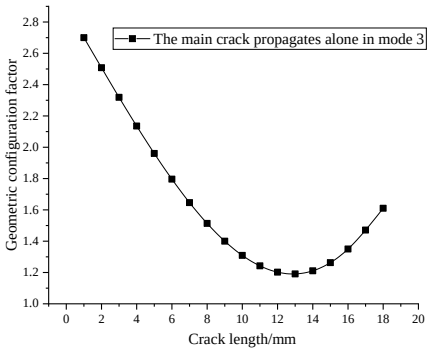

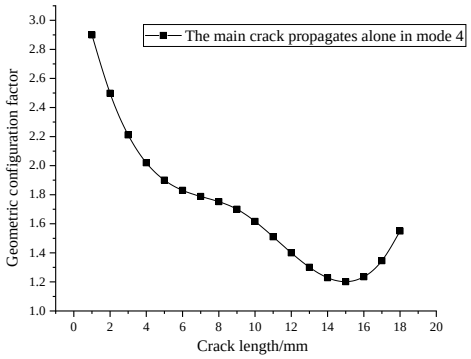

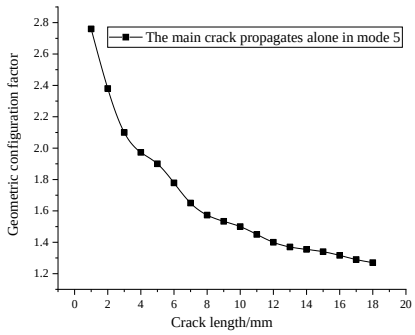

Figure2.5 Different modes under main Crack A, the geometric configuration factor change curve is extended separately

Geometric configuration factor with the expansion of the main crack presents two trends, it can be seen from the figure, with the expansion of cracks, geometric configuration factors decline and level off, but will soon be connected to the next hole and then began to rise, because the crack is closer to the hole, and the stress concentration of the hole edge. As can be seen from the figure2.5, the geometric configuration factor decreases gradually with the expansion of cracks.

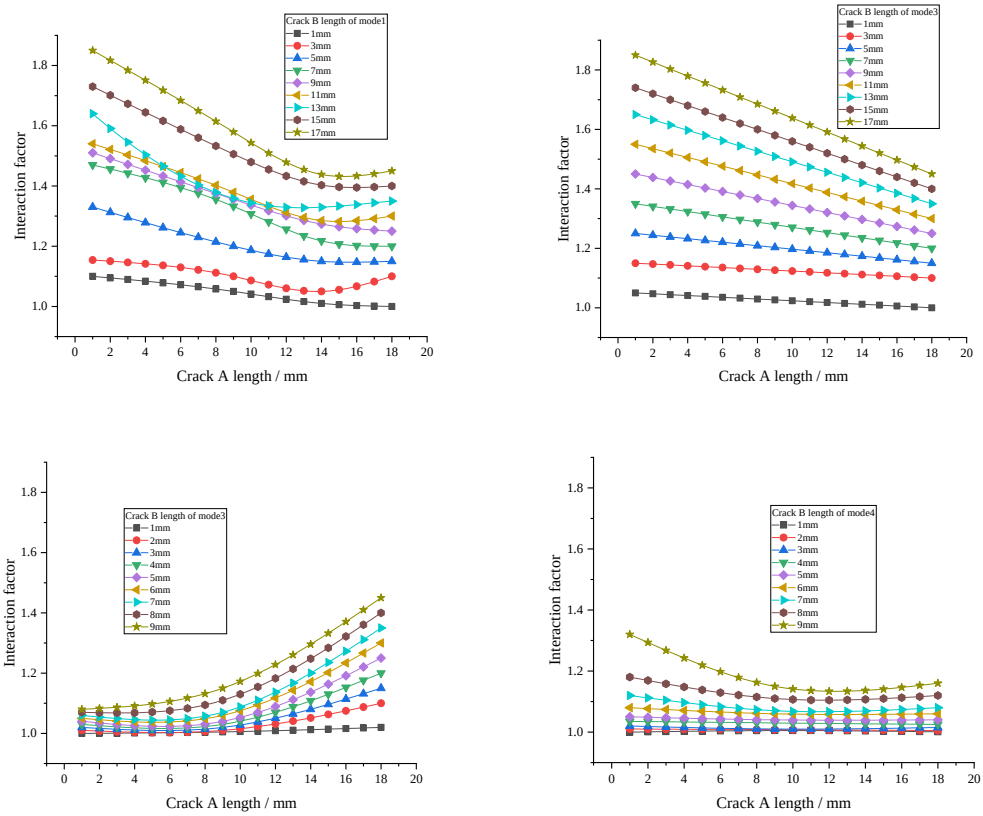

Figure2.6 Calculation results of mutual influence factors in different modes

As can be seen from the figure2.6, the interaction factor of cracks under mode 1 is up to

1.826, especially when primary crack A begins to expand the structure, this interaction is evident. As cracks get farther and farther apart, the interaction factors show a decreasing trend. The maximum interaction factor for cracks under mode 2 is 1.976, the interaction is very obvious. Mode 3 under Mutual Influence Factor as B Crack Expands, there is a growing trend. The maximum interaction factor for cracks under mode 4 is 1.372, the interaction is not obvious.

As can be seen from the figure2.7, the law of interaction caused by the change of main crack A in mode 5 with the change of crack B and crack C is more complex.

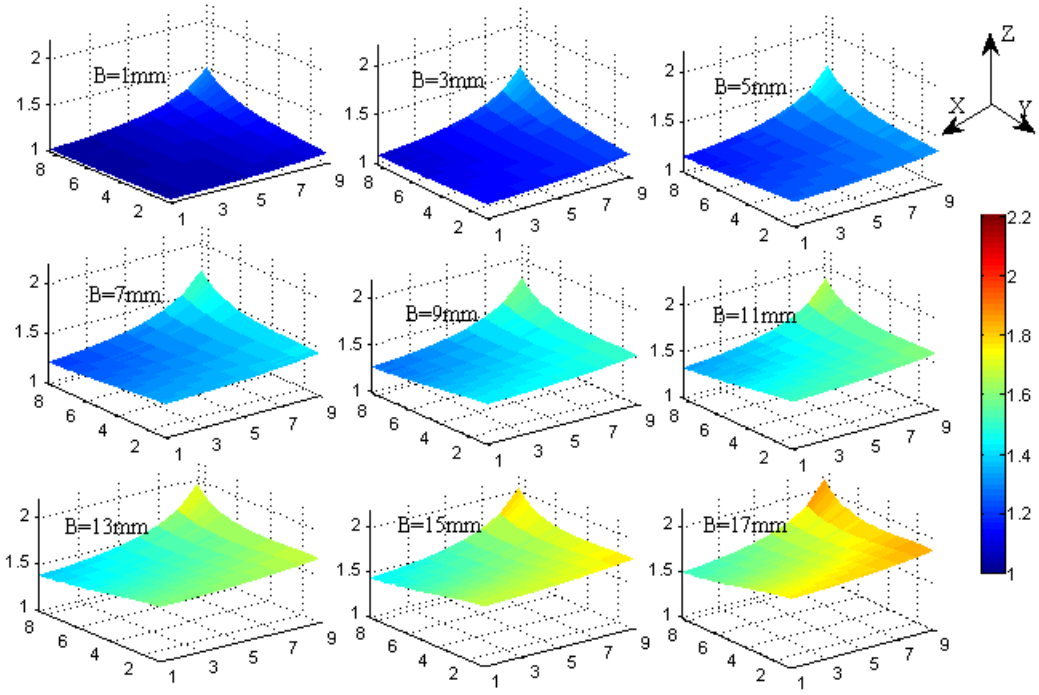

Figure2.7 Calculation result of mutual influence factor in mode 5

2.4 Conclusion

The interaction between multiple cracks has a great influence on crack expansion, and this chapter mainly studies the interaction between cracks in multi-site damage. Firstly, the basic solution method of crack tip interaction factor is introduced, and 5 crack modes are divided according to the different relative positions of cracks, on the basis of which the stress strength factor is obtained by finite factor analysis, and the interaction factor of crack tip is calculated.

Under the same test piece model, the following cracks affect each other by solving the interaction factors in 5 modes:

(a) Modes 1to 4 are the study of the interaction between the two cracks, it can be seen from the comparison, with the expansion from crack B, the interaction of crack tip will be more and more, as shown by the increase of mutual influence factors. This is due to the expansion from crack B, so that the main crack A assigned to the load increased, thus affecting the main crack stress intensity factor increase;

(b) The largest crack tip interaction factors under modes 1 to 4 are 1.826(from crack 17mm, main crack 1mm),1.976(from crack 17mm, main crack 1mm), 1.457(from crack 9mm, main crack 18mm),1.372(from crack 9mm, main crack 1mm). It can be seen that the crack tip under mode 3 affects each other by 5%, which can be regarded as the two cracks in practical applications without affecting modes 2 and 4 When the expansion from the crack exceeds 11mm, the interaction effect is more obvious, mode 1 The interaction between the lower cracks is very obvious;

(c) 2,3,4 modes, crack expansion does not connect, and as the main crack A expands, the interaction between cracks decreases gradually, due to the increasing distribution of loads to the entire structure as the main crack continues to expand, resulting in less force on the crack; The lower crack expansion is connected, and the crack expands quickly when connected. At this time, the interaction is mainly related to the distance between cracks;

(d) Mode 5 is a form of three crack extensions that can be seen as a combination of 1and3 modes. With the expansion of crack B, the mutual influence factor gradually increases, and the increment is more even, which is the same as the interaction of cracks under mode 3, as crack C expands, the interaction factor is gradually increasing, but the crack expands quickly in the final stage, and with the growth of main crack A, the interaction factor decreases gradually at the beginning of C crack, which conforms to the interaction of mode 1. However, when the length of the C crack exceeds 7mm, the interaction factors gradually increase, which is equivalent to the result of the joint action of the 1 and 3 patterns, and the influence of mode 3 on the interaction factors is relatively large.

3.1 Aircraft noise affects the design concept of soundproof windows for sensitive buildings in areas

With the development of China's aviation industry, the problem of environmental noise pollution caused by aircraft noise is becoming more and more serious, and the residents around the airport are more and more strongly affected by aircraft noise. Therefore, how to reduce the impact of aircraft noise on the lives, sleep, normal work and other aspects of the surrounding residents of theairport is an important environmental protectionissue.

The measures to prevent and control aircraft noise pollution are summarized into the following three categories: sound source noise reduction, transmission path noise reduction and noise sensitive building sound insulation measures. For the aircraft body, further noise reduction from the technical and economic feasibility of greater difficulties, short-term breakthrough can not be made. For noise reduction in transmission routes, the effective sound barrier for ground traffic noise such as roads and railways is not obvious for reducing aircraft noise. Therefore, the most effective and widely used measures in the prevention and control of aircraft noise pollution are to take sound insulation measures for noise-sensitive buildings, mainly to install soundproofing windows in noise-sensitive buildings.

3.1.1 Soundproof window calculation basis

Consider the sound of the exterior walls of sensitive buildings. The formula is as follows:

$$R_{tr\,A,C} > 10\lg\left(\frac{S_C}{S\times 10^{(L_{A1}-L_{A2}+10\lg\frac{S}{A})10}-S_q\times 10^{-RtrA,q/10}}\right)+K \quad (1)$$

in style,

RtrA, C - Soundproof window traffic noise insulation index, dB (A);

RtrA, q - Wall Traffic Noise Insulation Index, dB (A);

LA1 - Outdoor noise level, dB (A);

LA2 - Indoor allowed noise level, dB (A);

Sc - window area,m2;

A - average indoor sound absorption,m2;A is determined in accordance with Appendix B of the standard;

K - Design correction, in general K take 5.

Sq - exterior wall area,m2;

S - Room façade sound area, S-Sc-Sq (m2).

According to the standard requirements, the outdoor noise level of sensitive buildings is the A-level equivalent from the walls or windows of sensitive buildings.

3.1.2 The calculation of the soundproof index

In the laboratory simulation test, the laboratory for self-built brick mixed structure, wall and roof structure soundproofing to choose the general self-built building materials, the exterior wall is 24 cm solid brick wall, the roof is hollow floor, the external window surface is about 2.96 m2,the exterior wall area is about 9.6 m2,the room volume is about 54 m3 , part of the furniture in the room, the ground is cement. Aircraft noise LWECPN is 76.7 dB and soundproofing measures are required for sensitive buildings with LWECPN values greater than 75 dB, according to GB9660-1988. Based on the calculation formula in the previous section, you need to determine the value of the outdoor noise level of sensitive buildings. If the use of daytime, night equivalent A sound level, because the night aircraft aircraft is very uneven, resulting in a large difference in the impact of night aircraft noise, so the use of day, night equivalent A sound level can not fully take into account the impact of night flight, not representative. The measuring point LAeq, which has the greatest effect of aircraft noise during the day and night, is used to represent the outdoor noise level of sensitive buildings at 63 dBA and 61 dBA, respectively. The purpose of installing soundproofing windows or retrofitting soundproofing windows for sensitive buildings in areas affected by aircraft noise is to reduce the degree of distress about aircraft noise. The research shows that noise caused by different sound sources, different sound characteristics and different time is different, and a correction should be added to the measured or predicted sound level. Standard GB/T 3222.1-2006The Description, Measurement and Evaluation ofAcoustic Environmental Noise Part 1: Basic Parameters and Evaluation Methods specifies

the amount of corrections to the test sound level based on different sound sources, different sound characteristics and different time periods. The aircraft noise measurement sound level is modified from 3 dB to 6 dB, and the night measurement sound level is modified by 10 dB. Standard GB50118-2010 specification specifies a correction of aircraft noise of 3dB. Combined with the contents of the above two standards, the aircraft noise of the measuring point day and night the biggest impact of 1 hour equivalent A sound level LAeq was revised to 66 dBA, 74 dBA, respectively.

If it is necessary to find sensitive buildings sound insulation index day and night at the same time to meet the standard, should be calculated separately day and night noise peak hours required soundproofing window traffic noise insulation index, choose the larger of the two as the lowest design value. Therefore, the minimum design value for the sound insulation index for this measurement should be 37 dB.

Standard GB3096-2008 Sound Environmental Quality Standards stipulate that the noise limit for Category 4a areas is 70 dBA during the day, 55 dBA at night, noise bursts at night, the maximum sound level exceeds the ambient noise limit must not be higher than 15 dBA, so the maximum outdoor sound level limit at night is 70dBA, with reference to this rule, the maximum indoor noise allowable value should be 52dBA.

Table 3.1 The equivalent A sound level of aircraft noise for 1 hour

Time	L_{Aeq}/dBA	Plant times
00:00—1:00	46.7	0
1:00—2:00	50.4	1
2:00—3:00	46.6	0
3:00—4:00	45.5	0
4:00—5:00	46.1	0
5:00—6:00	50.0	0
6:00—7:00	53.0	3
7:00—8:00	55.1	3
8:00—9:00	56.5	8
9:00—10:00	60.0	16
10:00—11:00	61.5	21
11:00—12:00	62.0	22
12:00—13:00	61.2	20
13:00—14:00	61.3	21
14:00—15:00	60.6	17
15:00—16:00	62.1	22
16:00—17:00	63.0	23
17:00—18:00	60.3	18
18:00—19:00	60.1	16
19:00—20:00	60.9	18
20:00—21:00	61.2	19
21:00—22:00	60.1	16
22:00—23:00	61.0	20
23:00—24:00	56.9	6

4.1 Preparation of the passenger aircraft for flight

4.1.1 Principles for the preparation of aviation flight operations

In order to achieve an effective evaluation of the operation of airlines, it is necessary to have a comprehensive understanding of the indicators affecting the operation of airlines, but in the whole process of airline operations, there may be security factors for their operation monitoring, such as route conditions, airport security, air traffic conditions and weather conditions, while within the airline, its internal management will also have a certain impact on its operational supervision. Therefore, in the process of evaluating the operation of airlines, we must follow the principle of objectivity and practicability, and the evaluation system established must have a certain degree of scientific and comparability, which needs to be covered in the whole process.

4.1.1.1 Scientific principles

In the process of constructing the evaluation system, it is necessary to have some scientific, because only the results obtained by the scientific evaluation index system are true and reliable. However, the scientificity and rationality in the evaluation process are often influenced by the evaluation index, so it is necessaryto have a certain degree of scientificity in the process of evaluating the index construction. One of the first issues to be considered in the process of evaluating the construction of the index system is whether the overall structure of the index system is reasonable, and the safety factors existing in the process of airline operation monitoring need to be analyzed from multiple angles, and the selected indicators need to have some reliability and independence.

4.1.1.2 Principle of comprehensiveness

In the process of constructing the evaluation index system, each indicator should be integrated into the whole system for research, and the relevant indicators should not be separately studied, because there will inevitably be some links and effects within the different indicators, so it is necessary to start from the whole of all indicators for comprehensive consideration, if separated from the environment, the essence of the

indicators selected before will also change. At the same time, the selected indicators are not completely perfect, but if from the overall point of view, all the safety factors in the flight process of the aircraft to consider comprehensively, so that different factors can be combined, the airline's operational monitoring system for effective monitoring, the integrity of the entire evaluation index system will be greatly enhanced.

4.1.1.3 Principle of objectivity

Airlines' operation monitoring and evaluation system must also have a certain objectivity, only to ensure the objectivity and rationality of the evaluation index system can avoid the influence of some subjective factors and subjective understanding, make a reasonable evaluation of the monitoring level of aircraft operation, and make the necessary trade-offs according to the interaction between different indicators, to avoid some duplication and cross-cutting between different indicators, thus negatively affecting the subsequent evaluation work. At the same time, the evaluation index system can objectively and effectively reflect the overall situation, while ensuring that different indicators have certain authenticity and reliability.

4.1.1.4 Principle of Practicality

The most fundamental purpose of constructing the system of operational monitoring and safety assessment index of airlines is to provide the necessary reference for airlines to supervise their daily work, and also to provide the necessary reference for the macro-control of the Civil Aviation Authority. Therefore, in this paper, the author is to make a necessary assessment of the risks of airlines in the current stage of operation supervision. The selected indicators need to be highly overlapping with the daily operation of the airline, so as to provide the necessary basis for the daily management of the airline.

4.1.2 Operating environment

Aviation industry is a relatively special industry, in its operation process, the environment is a very important guarantee, at the same time in the aircraft set sail, landing and aircraft

operation process all need to meet certain standards, only in this way the aircraft's overall flight can be maintained in a stable state, so the operating environment in the safety assessment system is a very important factor. A careful analysis of the air crashes that have occurred in the current human history can be found that many major flight accidents are caused by the operation of the process, because the weather and other environments are too complex, so how to judge the weather in the course of the operation of the aircraft, while meeting the basic monitoring conditions under the premise of saving more costs for airlines worthy of further study. The secondary indicators of the aircraft's operating environment mainly include the following: weather conditions, route complexity, air traffic control factors, airport complexity, meteorological messages and so on.

4.1.2.1 Visibility

Aircraft are likely to be affected by different weather conditions during the flight process, and most flight accidents are caused by poor visibility, so visibility during the flight of the aircraft will bring greater restrictions, in all airports will be set the lowest take-off standards, and in the course of the flight will also be affected by various visibility factors, while landing at the airport will also be set minimum landing standards.

4.1.2.2 Complexity of the route

In general, the air route structure of aircraft is divided into city-to-route structure and hub route network structure, the rationality of air route is directly related to the scientific and rational use of air resources, only good route planning can effectively improve the efficiency of transportation, and only based on scientific and reasonable route planning, airlines can do a good job of route network manpower input, while different routes are not completely independent, there are certain mutual influence between different routes. At the same time, as mutual support exists, if airlines can do a good job of their own route structure planning, it can greatly reduce the air congestion and airport congestion, thereby significantly reducing security incidents, in addition, the route network structure planning and flight support and cross-station connectivity issues also have a closer relationship, so as to further affect the

operation and monitoring of airlines, Route network planning is an extremely important indicator in the process of risk assessment for airlines, and it must be paid high attention to. At present, most of our country's airlines' route structure is not exactly the same, some airlines use a network-like route structure, and some airlines use a point-to-point network structure. Therefore, there are large differences between the optimization routes between different routes, and due to weather and other factors, often lead to a large number of abnormal flights.

4.1.2.3 Air traffic control factor

In order to keep the operation of aviation in a safe and stable procedure, according to the aircraft flight process experienced in the region of division, can be divided into sub-tower control, near control, regional control, in general, air traffic control is a very complex system, China's current stage of air control experience is not very advanced, there are still many problems need to be further improved, air control can effectively ensure the safety of flight, At the same time, the flight condition can be maintained in a stable and efficient state, which greatly improves the efficiency of the use of air resources, effectively reduces the crowding and non-fluidity of air space. However, in different regions, the specific spatial environment is very different, so the specific control measures are not exactly the same, and the risks it monitors are not exactly the same. Although air command in general will not be directly related to the operation of airlines, but the control control personnel's own professional quality and professional ability for the operation also has a very large impact, therefore, in the evaluation system construction process must be taken into account.

4.1.2.4 Airport complexity

For airlines, the airport is the most important place for their operations, so the safety of the airport for the overall operation and supervision of airlines will have a very large impact, in recent years, China's aviation industry has been telling the development, almost every year there will be different degrees of accidents or accident symptoms, the number of occurrence is also increasing, so the safety of the airline operation assessment process must

examine the airport factors. However, in different airports, there are large differences in the environment, in addition to different airlines to implement the standards are not the same, the airport itself navigation equipment is not exactly the same, therefore, the impact on airlines is not exactly the same, in addition, aircraft in the airport is prone to bird-crash accidents, the airport's ground command will also have a greater impact on the operation and supervision of airlines. An investigation of the safety incidents that are data available at this stage reveals that most of the incidents occurred over the airport and over the airport.

4.1.2.5 Weather forecast

In the course of flight, the surrounding adverse weather conditions will have a greater impact on its visibility, such as fog, clouds, smoke, rain, snow and wind and sand, in addition to some extreme weather on the aircraft non-flight will also have a greater impact, such as typhoons, heavy rain, lightning strikes, etc. , if encountered in the course of operation of these weather conditions, while maintaining a minimum weather standards for a certain period of time, will cause certain obstacles to the normal flight of the aircraft, therefore, in such an environment, There are some hidden dangers in the operation of the aircraft, so if we want to fully guarantee the operation of the aircraft, we must make accurate predictions of these factors. The accuracy of weather forecast is measured, and the safety hazards existing in it are analyzed, and the relevant data in the statistical process are the average of airport statistics from the route. The evaluation criteria are: weather forecast=1- (airport weather forecast false positives/ airport weather forecasttimes) .

4.2 Analysis of the fit of the fuselage section of a passenger aircraft

In order to further study the fallability of typical metal body segments, this section will study the acceleration response, the overall energy change trend and the energy absorption characteristics of each structure during the crash of the fuselage segment.

4.2.1 Acceleration response

The acceleration response at the cabin seat of the fuselage is an important index to

evaluate the suitability of passenger aircraft, and the acceleration data is collected at the connection between the four seats and the floor, and the acceleration data is filtered by The Butterworth low-pass filter with a cut-off frequency of 20Hz according to NASA's experience. Figure 4.1 shows the acceleration response of the seat and floor connection during a crash in the fuselage segment of a typical metal passenger aircraft. The absolute value of the acceleration amplitude does not exceed 20g in the first 0.14s of the crash process. The maximum acceleration (approximately 28g) occurs at approximately 0.155s, the moment when the lower fuselage frame of the cabin strut and the fur collide with the ground (this article is called the secondary shock moment), due to the fact that the body is able to produce a large deformation at this time to absorb less energy structure, and the impact is transmitted directly from the cabin strut to the structure on the cabin floor. So while the fuselage segment is most affected when it hits the ground (i.e. 0s moments), the acceleration maximum occurs during the secondary shock. Comparing the four acceleration curves, the acceleration at the seat connection on the window side is usually greater than at the seat connection on the aisle side, as the window side structure is located in a triangular area consisting of floor and floor beams, body frames and skinning and cabin struts. It can be seen from the crash deformation diagram of the fuselage section that this area does not produce large structural damage and absorb energy due to the large stiffness during the crash, while the structure on the side of the aisle is located by the floor and floor beams, cabin struts, fuselage frames, skinning and cargo hold In the quad area of the lower structure, the lower structure of the cargo hold, the frame and the skin in the area during the crash will produce severe deformation and destruction and will be accompanied by a large amount of energy absorption, so the seat acceleration in the rigid triangle area is greater than that of other seats.

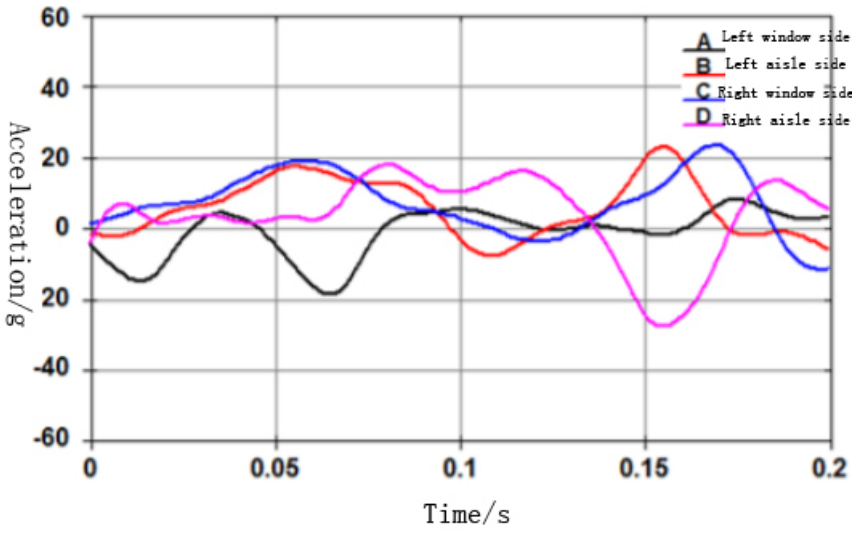

Figure 4.1 The acceleration response at the seat-to-floor connection

4.2.2 Energy conversion and energy absorption characteristics

During a crash, the impact energy consisting of the initial kinetic energy and the potential energy of the center of gravity that is squeezed will be converted into internal and frictional energy. The inner energy includes elastic and plastic deformation energy, frictional energy is generated by the self-contact of the fuselage components and the contact between the fuselage and the ground. Figure 4. 2 shows the trend of changes in kinetic and internal energy during a crash. The energy transition occurs from the moment the fuselage segment touches the ground. The slope of the energy curve is very large in the period from 0.0s to about 0.012s, as can be seen from the crash deformation diagram, in the initial stage of the crash, the fuselage frame and the skin of the lowest point of the fuselage section are broken, and the lower structure of the cargo hold also appears A certain degree of destruction, in this stage can produce deformation and absorb energy structure more, so the energy conversion efficiency is very high, and then to about 0.07s before the time period, the slope of the energy curve has a certain degree of reduction, during this stage the body frame and other structures can produce a limited amount of deformation, The efficiency of energy absorption is therefore also reduced, and the slope of the inner energy curve is very small over a period of time from approximately 0.07s to 0.128s, indicating that the energy conversion efficiency of this phase is very low, as there is little further structure such as the fuselage frame in the

lower part of the cargo hold The shape variable, except that the touch point of the fuselage segment moves all the way to both sides, and then, within the 0.162s period, the slope of the inner energy curve suddenly increases because the fuselage frame structure at the lower end of the cabin strut touches the ground and breaks and fails with a large amount of energy absorption. Therefore, the energy conversion efficiency of this stage is higher, and then the inner energy curve first appears a certain degree of decline, at which time the elastic energy of elastic deformation absorption is released, and finally the energy curve gradually stabilizes. The kinetic energy of the initial stage of the crash is about 16kJ, the internal energy of the 0.3s moment body segment is about 13kJ, the kinetic energy is about 1kJ, the remaining 2kJ energy is dissipated by friction, and the total energy conversion efficiency of the internal energy and friction energy is 93.75%.

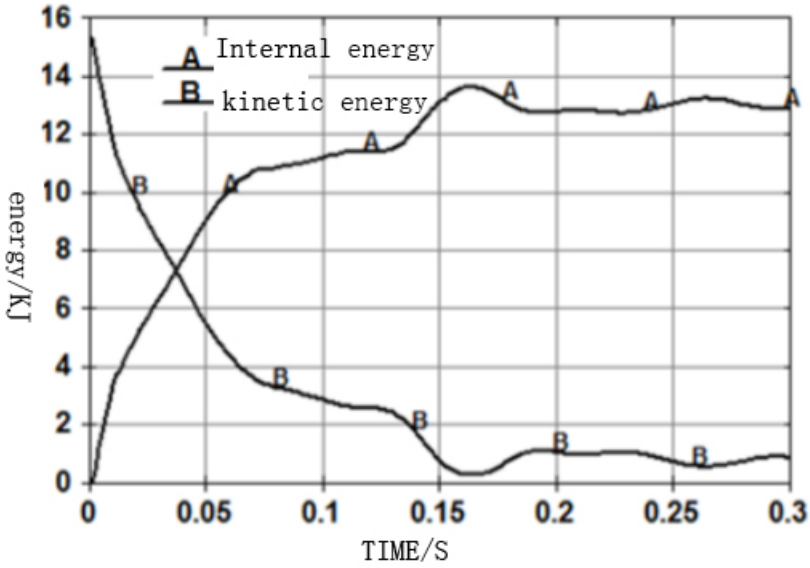

Figure 4.2 Trends in kinetic and internal energy

Compared with the experimental method, one of the significant advantages of finitenor method simulation crash is that the energy absorption of each structure and component can be recorded. This enables designers to quickly identify the most important energy absorption structures and assist in the design of structures that perform better. The fuselage segment consists of several substructures, such as skinning, frames, pillars, floors, floor beams, cargo floor components, etc. During a crash, each structure and component can absorb a portion of kinetic energy and convert it into internal energy. By analyzing the percentage of kinetic energy dissipated by individual structural components, it is possible to determine which

components play the most important role in the energy absorption during the crash process. Figure 4. 3 shows the energy absorption of different structures over time. The 0.3s moment frame, shear strip, skinning, cabin struts and lower cargo compartment structures absorb energy of 5.48kJ, 2.03kJ, 1.68kJ, 0.124kJ and 3 .21kJ, which absorbs a large amount of energy in the body frame, lower cargo compartment structure, shear strip plate and skinning, accounts for 44.7%, 26.2%, 16.6% and 13.7% of total internal energy, respectively. Frame is the main energy absorption structure in the process of crash, absorption accounted for nearly half of the total internal energy, cabin pillar absorption of energy is very small, because in order to ensure the cabin survival space considerations, the design strength of the pillar is greater, so in the production crash accident will not produce a larger deformation damage to play a role in energy absorption. During the initial phase of the crash, the energy curve slope of the frame, shear strip plate and skin is large, the absorption efficiency is higher, and then the slope of the three curves is reduced to a certain extent, and the energy absorption efficiency is reduced, while the energy curve of the lower structure of the cargo hold has a smaller slope change before 0.15s, and the absorption efficiency remains in a small range.

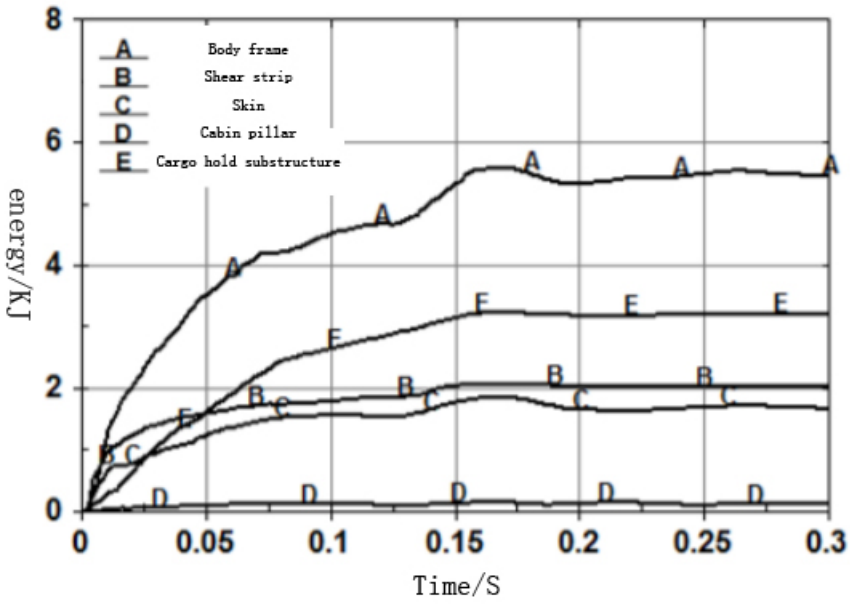

Figure 4.3 Trends in energy changes for each structure

GENERAL CONCLUSIONS

The following are the outcomes of my design work:

- preliminary design of a middle-range aircraft with 200 passengers;
- cabin layout of a middle-range aircraft with 200 passengers;
- calculations of the airplane's center of gravity;
- calculations of the landing gear's key geometrical parameters;
- choice of wheels that meet the requirements.

In the special part, the interaction between cracks in multi-point damage is studied. By solving the interaction factors of 5 modes, the following cracks affect each other:

- Modes 1 to 4 are the study of the interaction of two kinds of cracks. From the comparison, it can be seen that with the expansion of crack B, the interaction of the crack tips will increase, which is manifested as mutual increasing influence factors. This is because the expansion of crack B increases the load assigned to the main crack A, which affects the increase in the stress intensity factor of the main crack;

- The maximum crack tip interaction factor in modes 1 to 4 is 1.826 (crack 17mm, main crack 1mm), 1.976 (crack 17mm, main crack 1mm), 1.457 (crack 9mm, main crack 18mm), 1.372 (distance from crack) 9 mm, the main crack is 1 mm). It can be seen that the crack tips in mode 3 affect each other by 5%, which can be regarded as two cracks in practical applications, and have no effect on mode 2 and mode 4. When the crack propagation exceeds 11mm, the interaction effect is more obvious, mode 1 The interaction between the cracks in the lower layer is very obvious;

- In the 2,3,4 modes, the crack propagation is not connected. With the expansion of the main crack A, the interaction between the cracks gradually decreases. This is because as the main crack continues to expand, the load is distributed to the entire structure Increasing, resulting in less stress on the crack; the lower part of the crack propagates and connects, and the crack propagates faster during the connection. The interaction at this time is mainly related to the crack spacing;

- Mode 5 is three forms of crack propagation, which can be regarded as a combination of modes 1 and 3. With the expansion of crack B, the interaction factor gradually increases, and the increment is more uniform. This is the same as the interaction of cracks in mode 3. With the expansion of crack C, the interaction factor gradually increases, but the crack propagation is in the final stage Rapidly, as the main crack A grows, the interaction factor begins to gradually decrease in the C crack, which conforms to the mode 1 interaction. However, when the C crack length exceeds 7mm, the interaction factors gradually increase, which is equivalent to the result of the combined effect of mode 1 and mode 3. Mode 3 has a greater impact on the interaction factors.

REFERENCE

1. Froom P. Low back pain in pilots / P. Froom, J. Barzllay, Y. Catne, S. Margaliot // Aviation Space and Environment Medicine. – No.57, 1986. – P. 694-695.

2. Lusted M. Evaluation of the seating of Qantas flight deck crew. / M. Lusted, S. Healey, and J.A. Mandryk // Ergonomics. – No.25, 1994. – P. 275-282.

3. Sharma S. Static anthropometry: Current practice to determine aircrew aircraft compatibility / S. Sharma, K.S. Raju, A. Agarwal // Indian Journal of Aerospace Medicine. – No.51, 2007. – P. 40-47.

4. Sallinen S. Sleep, alertness and alertness management among commercial airline pilots on short-haul and long-haul flights / S. Sallinen, M., Mikael, K. Ketola // Accident Analysis &Prevention. – No.98, 2017. – P. 320-329.

5. Cohen D. An objective measure of seat comfort / Aviation, Space, and Environmental Medicine. – No.69, 1998. – P. 410-414.

6. Lin J F. Problems and improvements to airline SMS // World Maritime. – 1999.

7. Ma Z G. Civil Aviation Flight Safety Research // Chengdu: Southwest Jiaotong University – 2003.

8. Xu J, Wu B. Safety Management // Beijing: Aviation Industry Press – 1993. – P. 25-30.

9. Tan C Y. Airline Flight Safety Risk Assessment Study // China Civil Aviation Flight Academy – 2012

10. Liu D Y. Introduction to Civil Aviation // Civil Aviation Press of China – 2011.

11. Jackson K E, Fasanella E L. Crash simulation of a vertical drop test of a B737 fuselage section with overhead bins and luggage // Hapmton, Vriginia / NASA Langley Research Center – 2001.

12. Zhu X F, Feng Y W, Xue X F, et al. Evaluate the crashworthiness response of an aircraft fuselage section with luggage contained in the cargo hold. // International Journalof Crashworthiness. – 2017, 22(4). – P. 347-364.

13. Lavoie J A, Kellas S. Dynamic crush tests of energy-absorbing laminated composite plates // Composites Part A Applied Science & Manufacturing. – 1996, 27(6). – P. 467-475.

14. Ejackson K, Fasanella E L. Crash simulation of a vertical drop test of a commuter-class aircraft. // International Journal of Crashworthiness. – 2005, 10(2). – P. 173-182.

15. Fasanella E L, Jackson K E, Lyle K H. Finite element simulation of a full-scale crash test of a composite helicopter. // Journal of the American Helicopter Society. – 2002, 47(3). – P. 156-168.

16. Yu Z F, Gu H S, Wang H, et al. Crash simulation of the fuselage section with central wing box for a regional jet. // International Journal of Crashworthiness. – 2013, 18(1). – P. 19-28.

17. Chishti M, Wang C H, Thomson R S, et al. Numerical analysis of damage progression and strength of countersunk composite joints. // Composite Structures. – 2012, 94(2). – P. 643-653.

18. Elder D J, Verdaasdonk A H, Thomson R S / Fastener pull-through in a carbon fibre epoxy composite joint // Composite Structures. – 2008, 86(1). – P. 291-298.

19. Pearce G M, Johnson A F, Thomson R S, et al / Numerical investigation of dynamically loaded bolted joints in carbon fibre composite structures // Applied Composite Materials. – 2010, 17(3). – P.329-346.

20. Siromani D. Crashworthy design and analysis of aircraft structures. // Philadelphia / Drexel University. – 2013.

21. Jackson K E, Fasanella E L / Development and validation of a finite element simulation of a vertical drop test of an ATR42 regional transport airplane. // Hapmton, Vriginia / NASA Langley Rsearch Center. – 2008.

Appendix

INITIAL DATA AND SELECTED PARAMETERS

Passenger Number 190
Flight Crew Number 2
Flight Attendant or Load Master Number 5
Mass of Operational Items 1652.4
Payload Mass 22021.00

Cruising Speed 835
Cruising Mach Number 0.7784
Design Altitude 10.5
Flight Range with Maximum Payload 4075
Runway Length for the Base Aerodrome 2.55

Engine Number 2
Thrust-to-weight Ratio in N/kg 3.4000
Pressure Ratio 40.00
Assumed Bypass Ratio 11.00
Optimal Bypass Ratio 5.5
Fuel-to-weight Ratio 0.2800

Aspect Ratio 10.00
Taper Ratio 3.00
Mean Thickness Ratio 0.120
Wing Sweepback at Quarter Chord 28.0
High-lift Device Coefficient 0.84
Relative Area of Wing Extensions 0.00
Wing Airfoil Type
Winglets
Spoilers

Fuselage Diameter 4.20M
Finess Ratio 9.30

Horizontal Tail Sweep Angle 35.0
Vertical Tail Sweep Angle 40.0

CALCULATION RESULTS

Optimal Lift Coefficient in the Design Cruising Flight Point 0.42782

Induce Drag Coefficient 0.00915

ESTIMATION OF THE COEFFICIENT $D_m = M_{critical} - M_{cruise}$
Cruising Mach Number 0.77839
Wave Drag Mach Number 0.79078
Calculated Parameter D_m 0.01239
Wing Loading in kPa (for Gross Wing Area):
At Takeoff 5.065
At Middle of Cruising Flight 4.463
At the Beginning of Cruising Flight 4.886

Drag Coefficient of the Fuselage and Nacelles 0.00862
Drag Coefficient of the Wing and Tail Unit 0.00916

Drag Coefficient of the Airplane:
At the Beginning of Cruising Flight 0.02885
At Middle of Cruising Flight 0.02798

Mean Lift Coefficient for the Ceiling Flight 0.42782

Mean Lift-to-drag Ratio 15.29076

Landing Lift Coefficient 1.456
Landing Lift Coefficient (at Stall Speed) 2.184
Takeoff Lift Coefficient (at Stall Speed) 1.853
Lift-off Lift Coefficient 1.352
Thrust-to-weight Ratio at the Beginning of Cruising Flight 0.616
Start Thrust-to-weight Ratio for Cruising Flight 2.630
Start Thrust-to-weight Ratio for Safe Takeoff 3.068

Design Thrust-to-weight Ratio 3.190

Ratio $D_r = R_{cruise} / R_{takeoff}$ 0.857

SPECIFIC FUEL CONSUMPTIONS (in kg/kN*h):
Takeoff 26.9829
Cruising Flight 52.1849
Mean cruising for Given Range 57.6098

FUEL WEIGHT FRACTIONS:
Fuel Reserve 0.3391
Block Fuel 0.19610

WEIGHT FRACTIONS FOR PRINCIPAL ITEMS:
Wing 0.12728
Horizontal Tail 0.01115
Vertical Tail 0.01106
Landing Gear 0.04138
Power Plant 0.11315
Fuselage 0.08283
Equipment and Flight Control 0.12826
Additional Equipment 0.01184
Operational Items 0.01696
Fuel 0.23001
Payload 0.22606

Airplane Takeoff Weight 97413

Takeoff Thrust Required of the Engine 155.39

Air Conditioning and Anti-icing Equipment Weight Fraction 0.0222
Passenger Equipment Weight Fraction 0.0158
(or Cargo Cabin Equipment)
Interior Panels and Thermal/Acoustic Blanketing Weight Fraction 0.0068
Furnishing Equipment Weight Fraction 0.0135
Flight Control Weight Fraction 0.0058
Hydraulic System Weight Fraction 0.0162
Electrical Equipment Weight Fraction 0.0316
Radar Weight Fraction 0.0030
Navigation Equipment Weight Fraction 0.0045
Radio Communication Equipment Weight Fraction 0.0023
Instrument Equipment Weight Fraction 0.0053
Fuel System Weight Fraction 0.0068

Additional Equipment:
Equipment for Container Loading 0.0078
No typical Equipment Weight Fraction
(Build-in Test Equipment for Fault Diagnosis, 0.0040
Additional Equipment of Passenger Cabin)

TAKEOFF DISTANCE PARAMETERS

Airplane Lift-off Speed 278.57
Acceleration during Takeoff Run 2.60
Airplane Takeoff Run Distance 1147
Airborne Takeoff Distance 578
Takeoff Distance 1725

CONTINUED TAKEOFF DISTANCE PARAMETERS

Decision Speed 264.64
Mean Acceleration for Continued Takeoff on Wet Runway 0.47
Takeoff Run Distance for Continued Takeoff on Wet Runway 1647.59
Continued Takeoff Distance 2225.97m
Runway Length Required for Rejected Takeoff 2305.06m

LANDING DISTANCE PARAMETERS

Airplane Maximum Landing Weight 82789
Time for Descent from Flight Level till Aerodrome Traffic Circuit Flight 20.8
Descent Distance 48.32
Approach Speed 266.15
Mean Vertical Speed 2.12
Airborne Landing Distance 523
Landing Speed 251.15
Landing run distance 870
Landing Distance 1393
Runway Length Required for Regular Aerodrome 2327
Runway Length Required for Alternate Aerodrome 1978